Food antigen-specific Type 1 Regulatory T cells induced by intestinal epithelial cells maintain food tolerance

Tingyue Zhou[1#], Guorong Zhang[1#], Yan Wang[1], Wei Jiang[1], Chenyang Wu[1], Runzhi Li[1], Tingting Wan[1], Yucai Wang[1], Andrew James Macpherson[1,2], Shu Zhu[*1,2]

The intestinal epithelium serves as the primary barrier to dietary antigens, yet its role in establishing oral tolerance remains incompletely understood. In particular, how antigen presentation by intestinal epithelial cells (IECs) shapes antigen-specific T cell responses to dietary antigens is not fully resolved. Here we demonstrate that IECs induce the differentiation of FOXP3$^-$IL-10$^+$ Type 1 regulatory (Tr1) cells in response to specific dietary antigens. Food antigen-specific T cells are initially primed in gut-draining lymph nodes before migrating to the small intestinal lamina propria (siLP). Within the small intestine, these cells receive cognate antigen presented by IECs, which programs their differentiation into Tr1 cells. The maintenance of this Tr1 phenotype requires continuous, antigen-specific engagement with IECs. Targeted delivery of allergen epitopes to IECs using nanoparticle carriers induces antigen-specific Tr1 cells and protects against food allergy in a murine model. These findings establish IEC-directed Tr1 induction as an additional mechanistic basis for oral tolerance and offer a novel, targeted strategy for food allergy immunotherapy.

https://doi.org/10.15302/vita.2026.08.0066

INTRODUCTION

The human small intestinal mucosa, with a surface area of up to 30 square meters, is continuously exposed to a vast array of food-derived antigens. To prevent unnecessary inflammatory responses against these non-self yet harmless entities, which are collectively considered xenobiotics, the intestinal immune system must establish and maintain robust oral tolerance[1,2].

Intestinal antigen-presenting cells (APCs) play pivotal roles in this process. Lamina propria-resident CX3CR1$^+$ macrophages sample luminal antigens via transepithelial dendrites and transfer them to dendritic cells (DCs)[3]. Migratory CD103$^+$ conventional DCs (cDCs) then traffic from the mucosa to the mesenteric lymph nodes (mLNs), where they drive the differentiation of food antigen-specific FOXP3$^+$ regulatory T cells (Tregs)[4-6]. More recently, a specialized population of RORγt$^+$ APCs has been identified as uniquely essential for the robust induction of such dietary antigen-specific Tregs[6-9].

Beyond professional APCs, small intestinal epithelial cells (IECs) also express MHCII and shape the local CD4$^+$ T cell populations[10-13]. Our previous work demonstrated that loss of IEC-mediated antigen presentation predisposes mice to food allergy[14]. Furthermore, MHCII expression on IECs is required for the generation of food-reactive CD4$^+$CD8αα$^+$ intraepithelial lymphocytes (IELs)[15,16]. Collectively, these findings implicate IEC antigen presentation in oral tolerance, yet direct evidence that IECs present dietary antigens to induce specific, tolerogenic T cell responses has remained lacking.

Several CD4$^+$ T cell populations with regulatory potential originate from the mLNs and home to the small intestine to mediate tolerance to food antigens[5,17,18]. While the role of FOXP3$^+$ Tregs in food tolerance is well established[19,20], other subsets, including Th^{lin-} cells[17] and CD4$^+$CD8αα$^+$ IELs[16,21], have also been reported to respond to dietary antigens. Among these, FOXP3$^-$IL-10$^+$ Type 1 regulatory (Tr1) cells represent a distinct population enriched in the small intestine rather than the colon, mirroring the distribution of food antigen[22]. Their numbers oscillate with daily food intake, suggesting a link to feeding[11]. Although Tr1 cells have been implicated in models of colitis[23], tumor immunity[24], type 1 diabetes[25] and experimental autoimmune encephalomyelitis[26], direct evidence supporting a physiological role for Tr1 cells in tolerance to specific dietary antigens has been lacking. Although a recent study suggested that small intestinal T-bet$^+$ "Tr1" cells are influenced by food antigen[27], whether these cells produce IL-10 *in vivo* (a defining criterion for their designation as Tr1 cells) and whether *bona fide* Tr1 cells in the small intestine directly recognize food antigen remain unclear.

Here, we demonstrate that small intestinal FOXP3$^-$IL-10$^+$ Tr1 cells respond to food antigens presented by IECs. Food antigen-specific T cells are first primed by professional APCs in mLN and then migrate to the small intestinal lamina propria (siLP), where they are re-stimulated by IECs and acquire the regulatory Tr1 cell phenotype. Harnessing this pathway, we show that nanoparticle-mediated delivery of

1. State Key Laboratory of Immune Response and Immunotherapy, School of Basic Medical Sciences, Division of Life Sciences and Medicine, University of Science and Technology of China, Hefei, Anhui, China. 2. Department of Digestive Disease Institute, The First Affiliated Hospital of USTC, Division of Life Sciences and Medicine, University of Science and Technology of China, Hefei, Anhui, China. #These authors contribute equally. *Correspondence: Shu Zhu (zhushu@ustc.edu.cn)
Received: June 20, 2026; Accepted: August 26, 2026; Published: September 15, 2026

synthetic peanut peptides to IECs induces antigen-specific Tr1 cells and prevents peanut allergy, revealing a novel strategy for immunotherapy.

RESULTS

Small intestinal Tr1 cells respond to dietary antigen

In addition to FOXP3$^+$ Tregs, FOXP3$^-$IL-10$^+$ Tr1 cells represent another CD4$^+$ T cell subset with regulatory properties in the siLP. While Tregs were broadly distributed across lymphoid and mucosal tissues (Supplementary Fig. S1a–d), Tr1 cells selectively accumulated in the siLP and were largely absent from 34 other tissues examined (Supplementary Fig. S1a–d). Given that food antigens are abundant in the small intestine, and that Tr1 cells are reduced in mice with disrupted circadian feeding rhythms[11] or with Gasdermin D mutations where dietary antigens fail to induce IEC MHCII expression[14], we hypothesized that Tr1 cells may be specialized to respond to food-derived antigens.

We first evaluated the influence of food antigens on these regulatory cell populations in IL-10^{GFP}/FOXP3^{RFP} dual reporter mice. To achieve this, we utilized a specifically formulated amino acid diet (AAD) lacking proteinaceous food antigens, and compared it to a synthetic casein diet (CAD). We deliberately selected this synthetic CAD as a rigorous control because it is compositionally identical to the AAD, differing only in the presence of intact proteins (beta-casein and kappa-casein) rather than free amino acids (Supplementary Fig. S2a, b). Surprisingly, while Treg numbers in the siLP remained unchanged, Tr1 cells were almost completely absent in AAD-fed mice (Fig. 1a). This effect was specific to the small intestine, as Tr1 and Treg populations in the colonic lamina propria (cLP) were unaffected (Fig. 1a). These data suggested that Tr1 cells, rather than Tregs, depend on dietary antigens for their maintenance in the siLP.

To compare the antigen specificity of these two populations, we sorted Tr1 and Treg cells from CAD-fed mice and performed single-cell RNA and TCR sequencing (Fig. 1b, c). After demultiplexing, of 9,028 recovered cells, 4,870 (53.94%) were Tr1 and 4,158 (46.06%) were Treg, consistent with their *in vivo* ratios (Supplementary Fig. S1b). The cells were annotated based on their specific gene expression profiles and then clustered to 14 cell populations in an unsupervised manner (Fig. 1b). Within the sorted Tr1 cells, 70.03% expressed *Il10*, *Ifng* and the marker of CD4$^+$ T cell anergy[28] as well as co-inhibitory molecules such as *Pdcd1* and *Lag3*. These cells are referred to as typical Tr1 cells (Fig. 1b; Supplementary Fig. S3a,b). The remaining Tr1 cells co-expressed *Il10* with *Il17a* or *Il4*, suggesting potential transitional states[29,30]. Tregs segregated into two clusters based on *Rorc* expression (Fig. 1b). Except for the proliferating cell cluster composed of both Tr1 cells (53.98%) and Treg cells (46.02%), the other cell clusters were either predominantly Tr1 cells (clusters 1–9) or predominantly Treg cells (clusters 10–13) (Fig. 1b), indicating that these two cell populations exhibit obvious transcriptional differences. Compared with Treg cell subsets, typical Tr1 cell subsets have higher expression levels of *Ccl5*, *Gzmk* and *Prf1* (encoding perforin) and lower expression levels of *Il2ra*, *Cd200* and *Tnfsf8*, which is consistent with the characteristics of Tr1 cells described in previous studies[24].

TCR repertoire analysis revealed striking differences. Typical Tr1 cells displayed larger clone sizes than Tregs (Fig. 1c; Supplementary Fig. S3c), suggesting recognition of a more focused antigen pool. Remarkably, TCR clonotypes were almost never shared between typical Tr1 cells and Tregs, with sharing confined to the proliferating cluster (Fig. 1d). Cells sharing identical TCRs clustered together (Supplementary Fig. S4), reinforcing that Tr1 and Treg cells in the siLP have distinct antigen specificities.

To directly test whether Tr1 cells recognize dietary antigens, we sorted Tr1 and IL-10$^+$ Treg cells from the siLP of CAD-fed mice and co-cultured them with APCs loaded with casein protein (Fig. 1e). Tr1 cells, but not Tregs, were activated by both intact and digested casein (Fig. 1f; Supplementary Fig. S3d). These results demonstrate that Tr1 cells and Treg cells in the siLP possess distinct antigen specificities, and that Tr1 cells are activated by food-derived antigens.

We next asked whether this phenomenon is unique to casein. Mice fed a synthetic whey-based diet (WHD; containing no detectable casein; Supplementary Fig. S2a–c) also exhibited robust Tr1 enrichment (Supplementary Fig. S5a). Similarly, mice fed a standard grain-based diet (GBD; protein from soybean and fish meal, no added casein; Supplementary Fig. S2c–e) showed abundant Tr1 cells in the siLP, in contrast to AAD-fed controls (Supplementary Fig. S5b). Re-analysis of a published scRNA-seq dataset[16] confirmed that FOXP3$^-$IL-10$^+$ Tr1 cells were present in GBD-fed mice but absent in AAD- or AAD+ovalbumin (OVA)-fed mice (Supplementary Fig. S5c,d). Together, these findings demonstrate that Tr1 cell induction is a generalized response to dietary proteins, not restricted to specific antigens like casein.

Tr1 cells recognize dietary antigen presented by IECs

Given that MHCII expression on IECs is critical for food tolerance[14] and generating food-reactive T cells[15,16], we hypothesized that IEC-mediated antigen presentation might drive the differentiation of dietary antigen-specific Tr1 cells. To test this, we crossed *H2-Ab1*$^{\Delta IEC}$ mice with IL-10^{GFP}/FOXP3^{RFP} dual-reporter mice. Strikingly, loss of MHCII on IECs led to an almost complete disappearance of Tr1 cells in the siLP under CAD-fed conditions (Fig. 2a), phenocopying the effect of protein-free AAD feeding in wild-type mice (Fig. 1a). This indicated that IEC antigen presentation is required for Tr1 cell development.

We next asked whether IECs can present food antigens to Tr1 cells. We performed mass spectrometry (MS) to evaluate the peptides bound to MHCII molecules that expressed on EpCAM$^+$CD45$^-$ IECs sorted from the small intestine of CAD-fed *H2-Ab1*$^{f/f}$ mice (Fig. 2b). IECs sorted from CAD-fed *H2-Ab1*$^{\Delta IEC}$ mice or AAD-fed *H2-Ab1*$^{f/f}$ mice were used as negative controls (Fig. 2b). The peptide lengths identified in IEC MHCII immunopeptidome were normally distributed between 12 and 20, and with a median length of 15–16 amino acids (Fig. 2c; Supplementary Fig. S6a, Table S1). IECs from CAD-fed *H2-Ab1*$^{f/f}$ mice yielded the highest number of MHCII-bound peptides, whereas few peptides were recovered from AAD-fed controls, and those from *H2-Ab1*$^{\Delta IEC}$ mice were attributed to non-specific background (Fig. 2c). The core binding motif of the MHCII-bound peptides from IECs derived from CAD-fed *H2-Ab1*$^{f/f}$ mice and AAD-fed *H2-Ab1*$^{f/f}$ mice, but not from CAD-fed *H2-Ab1*$^{\Delta IEC}$ mice, matched the canonical motif of the

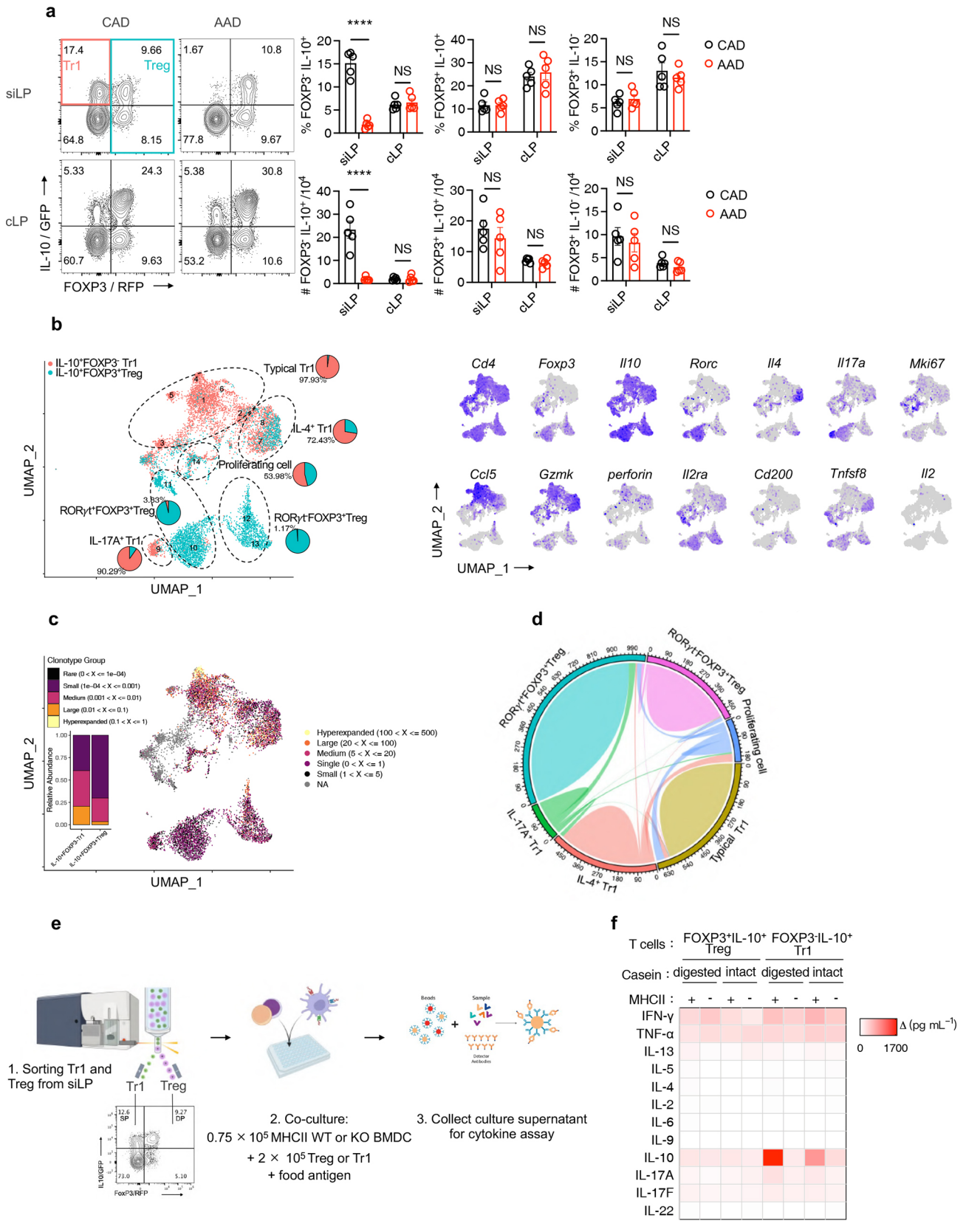

Fig. 1 Tr1 cells in siLP respond to dietary antigen. a Representative FACS plots and quantifications of FOXP3 and IL-10 expression on gated CD45$^+$CD3$^+$CD4$^+$ T cells isolated from the siLP and cLP of mice fed with CAD or AAD (n = 5). **b–d** Single-cell RNA and TCR sequencing of FOXP3$^-$IL-10$^+$ Tr1 cells and FOXP3$^+$IL-10$^+$ Treg cells isolated from the siLP of mice fed with CAD. Tr1 and Treg cells were isolated from two mice, pooled by cell type, labeled with distinct Hashtags, and sequenced together in a single batch. Uniform Manifold Approximation and Projection (UMAP) plot of the cells, with clusters annotated into 6 cell types. The pie chart next to each cluster shows the cellular composition of that cluster (**b**, left). Single-cell expressions of the indicated genes were projected on the UMAP plot (**b**, right). **c** TCR clonotype size

distribution projected onto the UMAP plot. TCR clonotype abundance of Tr1 cells or Treg cells was quantified on a bar graph. **d** Circos plots showing TCR clonotypes shared between each annotated cell type. Each link shows how many T cells in that cell type have a shared TCR. **e**, **f** FOXP3$^-$IL-10$^+$ Tr1 cells or FOXP3$^+$IL-10$^+$ Treg cells were isolated from the siLP of CAD-fed mice and co-cultured with *H2-Ab1*$^{+/+}$ or *H2-Ab1*$^{-/-}$ bone marrow-derived DCs (BMDCs) in the presence of digested or intact casein proteins. After 24 h, culture supernatants were collected for cytokine analysis. Schematic diagram of the co-culture experiment (**e**). Measurement of T cell cytokine production in the co-culture experiment (**f**). The heatmap displays the mean of three replicates, and the raw data are presented in Supplementary Fig. S3d. Data are representative of at least three independent experiments (**a**, **f**). Data are mean ± SEM and were analyzed by two-way ANOVA with Šídák's multiple comparisons test (**a**), NS, no significance; $^{****}P < 0.0001$.

H2-Ab1 allele[31] (Supplementary Fig. S6b), confirming genuine MHCII loading.

Importantly, eight food-derived peptides were identified exclusively in IECs from CAD-fed *H2-Ab1*$^{f/f}$ mice (Fig. 2d; Supplementary Fig. S6c). These peptides mapped to two regions of casein — $Cb_{70–84}$ and $Cb_{95–112}$ — both predicted to bind MHCII with high affinity[31,32] (Fig. 2d). Thus, IECs present defined casein epitopes.

Given that multiple dietary contexts induce Tr1 cells, we tested whether IEC-MHCII presents a broader spectrum of food antigens. Feeding a GBD to *H2-Ab1*$^{\Delta IEC}$ mice resulted in a marked Tr1 deficiency (Supplementary Fig. S7a), confirming that IEC-MHCII is essential even with complex diets. Immunopeptidomic analysis of IECs from GBD-fed mice identified three food-derived peptides from fish-meal myosin heavy chain (*Coilia grayii*), which were absent in *H2-Ab1*$^{\Delta IEC}$ and AAD-fed controls (Supplementary Fig. S7b–e and Table S2). These peptides exhibited high predicted MHCII affinity and mapped to regions divergent from the murine homolog, confirming their exogenous origin (Supplementary Fig. S7e). Collectively, these findings demonstrate that IECs present a broad spectrum of dietary antigens, not merely casein.

We next investigated whether dietary antigen presented by IECs could be recognized by the TCR characterized by the aforementioned single-cell TCR sequencing dataset. We retrieved paired TCR sequences from the 133 most expanded Tr1 cell or Treg cell clones (Fig. 1c). We then cloned these TCRs into NFAT-GFP 58α$^-$β$^-$ T cell hybridoma cell line and tested their response toward eight food-derived peptides identified in our IEC MHCII immunopeptidome (Fig. 2b–d). Among the 61 TCRs from typical Tr1 cells, 6 TCRs could respond to the peptide mixture (Fig. 2e; Supplementary Fig. S4a), while the remaining TCRs showed no obvious activation; whereas none of the 72 Treg TCRs responded to the peptide mixture (Fig. 2e; Supplementary Fig. S4a). Individual peptide testing revealed that one Tr1 TCR recognized $Cb_{70–84}$, while the remaining five responded to the $Cb_{95–112}$ region. Among these, the Cb4-7 TCR showed the strongest response to the $Cb_{98–112}$ epitope (Fig. 2e; Supplementary Fig. S4b).

To validate these findings *in vivo*, we generated $Cb_{98–112}$-loaded MHCII tetramers. Equal numbers of polyclonal Tr1, Treg, and FOXP3$^-$IL-10$^-$ cells were sorted from the siLP of CAD-fed reporter mice and stained with the tetramer (Supplementary Fig. S8a,b). $Cb_{98–112}$ tetramer$^+$ cells were abundant among Tr1 cells but rare among Tregs or FOXP3$^-$IL-10$^-$ cells (Fig. 2f). As a control, Tr1 cells from WHD-fed mice — which maintain normal IEC MHCII expression (Supplementary Fig. S8c) and Tr1 frequencies (Supplementary Fig. S5a) but lack casein exposure — showed no tetramer staining (Fig. 2f). Together, these results demonstrate that Tr1 cells specifically recognize dietary antigen epitopes presented by IECs.

IECs maintain IL-10 expression by Tr1 cells

The loss of MHCII on IECs reduced the frequency of FOXP3$^-$ IL-10$^+$ Tr1 cells while increasing the proportion of FOXP3$^-$IL-10$^-$ cells in the siLP, without altering total CD4$^+$ T cell numbers (Fig. 2a; Supplementary Fig. S9a). This suggested that IEC antigen presentation might be required for maintaining IL-10 expression. To test this, we sorted Tr1 cells and IL-10$^+$ Tregs from the siLP of CAD-fed dual-reporter mice and cultured them *in vitro* (Fig. 2g). Tr1 cells rapidly lost IL-10 expression within 12 h, whereas Tregs remained stable (Fig. 2h). However, when Tr1 cells were co-cultured with IECs from CAD-fed mice, IL-10 expression was rescued (Fig. 2h, i). In contrast, co-culture with MHCII-deficient IECs or with IECs from WHD-fed mice (lacking cognate casein antigen) failed to maintain IL-10 expression (Fig. 2h, i). Thus, sustaining Tr1 IL-10 production *in vitro* requires both IEC antigen presentation and the presence of cognate antigen.

To determine whether IEC antigen presentation maintains Tr1 IL-10 expression *in vivo*, we generated *H2-Ab1*^{Vil1CreERT2} mice — by crossing *H2-Ab1*$^{f/f}$ mice (already crossed with IL-10^{GFP}/FOXP3^{RFP} dual reporter mice) with *Vil1*^{CreERT2} mice — enabling tamoxifen-inducible deletion of MHCII specifically in IECs (Fig. 2j). Tamoxifen treatment of control *H2-Ab1*$^{f/f}$ mice had no effect on Tr1 cells or casein-specific ($Cb_{98–112}$ tetramer$^+$) T cells (Supplementary Fig. S9b, c). In contrast, tamoxifen-treated *H2-Ab1*^{Vil1CreERT2} mice exhibited: a reduction in total polyclonal Tr1 cells (Supplementary Fig. S9d); a decrease in the proportion of casein-specific T cells within the Tr1 gate; and a corresponding increase in casein-specific FOXP3$^-$IL-10$^-$ cells (Fig. 2k). Notably, the total number of casein-specific T cells remained unchanged (Fig. 2k), indicating that antigen-specific cells downregulated IL-10 expression upon loss of IEC MHCII, rather than being deleted or failing to differentiate.

Collectively, these data demonstrate that IEC-mediated antigen presentation maintains IL-10 expression in Tr1 cells both *in vitro* and *in vivo*, revealing a dynamic and ongoing requirement for cognate antigen encounter to preserve the Tr1 phenotype.

Circadian migration enables Tr1 cells to interact with IECs

Given that the TCRs recognizing IEC-presented antigens originate from Tr1 cells in the siLP, we next explored the anatomical basis of T cell–IEC interactions. Profiling the intraepithelial lymphocyte (IEL) compartment of IL-10^{GFP}/FOXP3^{RFP} dual-reporter mice revealed a population of conventional CD4$^+$IL-10$^+$ T cells distinct from Tregs (Supplementary Fig. S10). The frequency of this IL-10$^+$ cell population was highly rhythmic, peaking at Zeitgeber Time (ZT) 2 and reaching a nadir at ZT14, consistent with previous reports[11]. However, no circadian rhythm-dependent IL-10 expression was

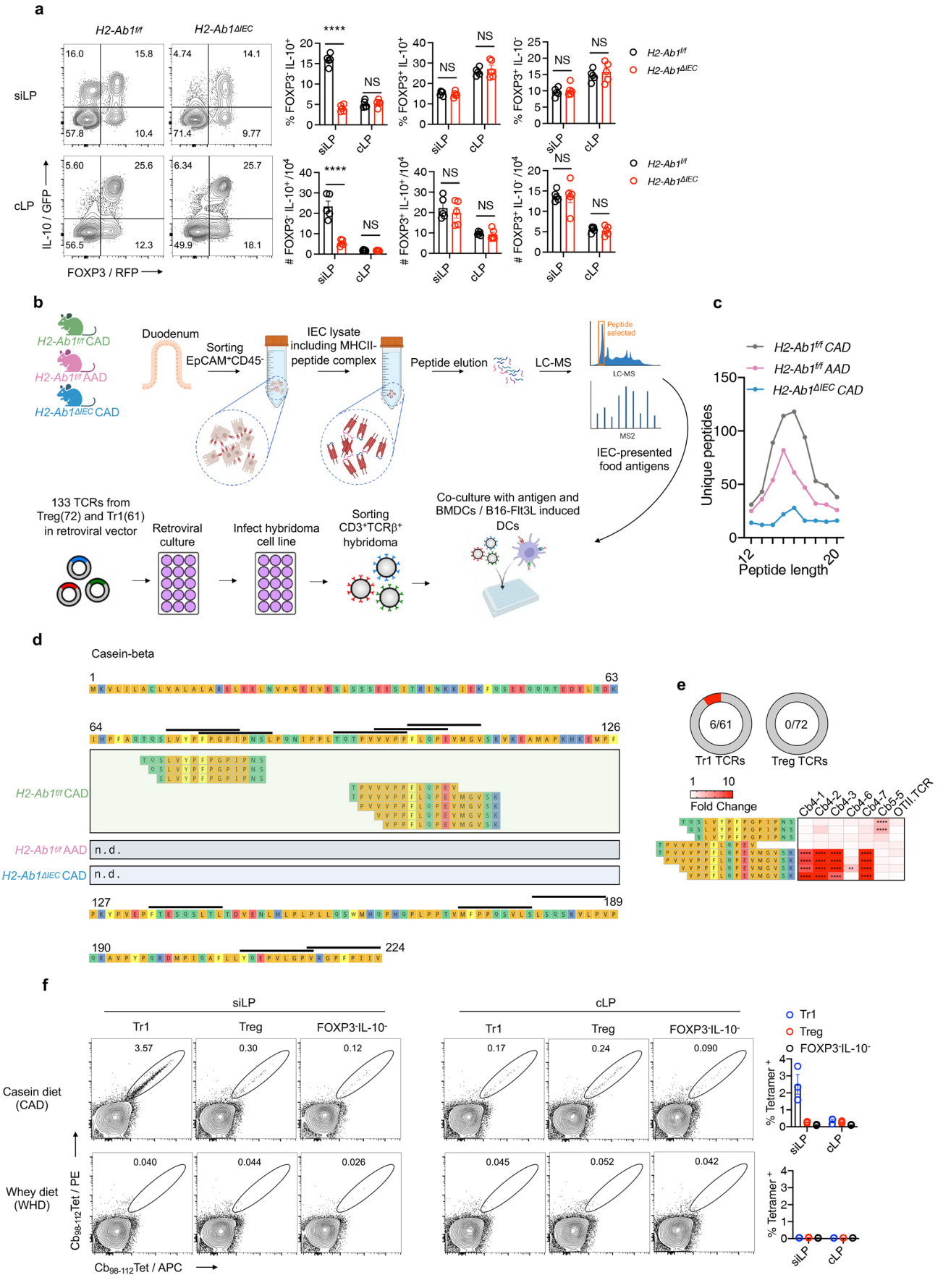
a
H2-Ab1f/f
H2-Ab1ΔIEC
siLP
cLP
IL-10 / GFP
FOXP3 / RFP
16.0
15.8
57.8
10.4
4.74
14.1
71.4
9.77
5.60
25.6
56.5
12.3
6.34
25.7
49.9
18.1
% FOXP3- IL-10+
% FOXP3+ IL-10+
% FOXP3+ IL-10-
# FOXP3- IL-10+ /10^4
# FOXP3+ IL-10+ /10^4
# FOXP3+ IL-10- /10^4
****
NS
b
H2-Ab1f/f CAD
H2-Ab1f/f AAD
H2-Ab1ΔIEC CAD
Duodenum
Sorting EpCAM+CD45-
IEC lysate including MHCII-peptide complex
Peptide elution
LC-MS
Peptide selected
MS2
IEC-presented food antigens
133 TCRs from Treg(72) and Tr1(61) in retroviral vector
Retroviral culture
Infect hybridoma cell line
Sorting CD3+TCRβ+ hybridoma
Co-culture with antigen and BMDCs / B16-Flt3L induced DCs
c
H2-Ab1f/f CAD
H2-Ab1f/f AAD
H2-Ab1ΔIEC CAD
Unique peptides
Peptide length
d
Casein-beta
H2-Ab1f/f CAD
H2-Ab1f/f AAD
H2-Ab1ΔIEC CAD
n.d.
e
6/61
Tr1 TCRs
0/72
Treg TCRs
Fold Change
Cb4-1
Cb4-2
Cb4-3
Cb4-6
Cb4-7
Cb5-5
OTII.TCR
f
siLP
cLP
Tr1
Treg
FOXP3-IL-10-
Casein diet (CAD)
Whey diet (WHD)
3.57
0.30
0.12
0.17
0.24
0.090
0.040
0.044
0.026
0.045
0.052
0.042
% Tetramer+
Cb98-112Tet / PE
Cb98-112Tet / APC

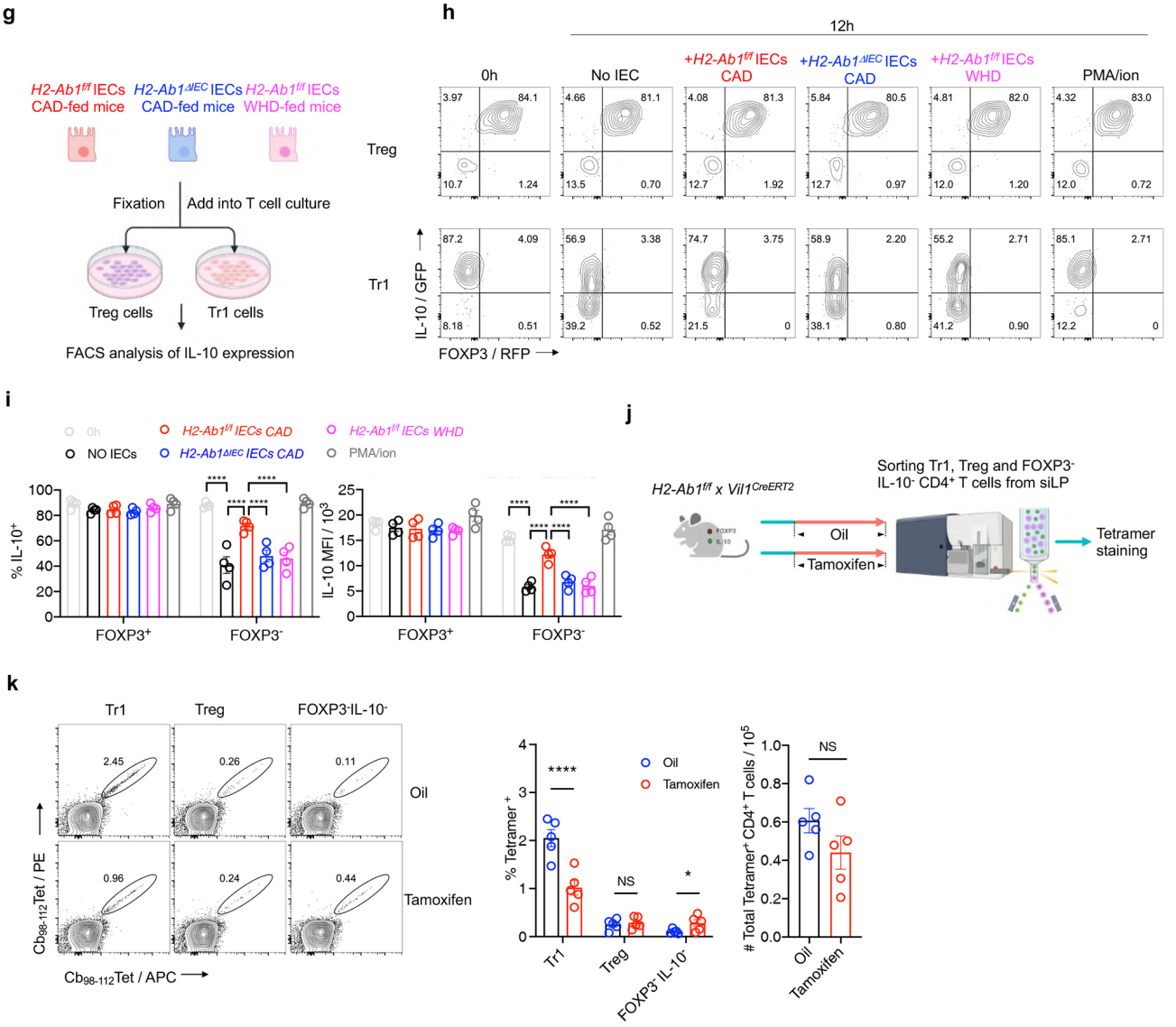

Fig. 2 Tr1 cells recognize dietary antigen presented by IECs. a Representative FACS plots and quantification of FOXP3 and IL-10 expression on gated $CD45^+CD3^+CD4^+$ T cells isolated from the siLP and cLP of the indicated mice ($n = 5$). **b–e** IEC MHCII peptidome identifying dietary antigens recognized by Tr1 or Treg cell TCRs. **b** Schematic diagram of the experiment. MHCII peptidome analysis was performed on IECs isolated from the indicated mice (a total of 5×10^7 cells pooled from 2 mice per group). TCRs from the TCR repertoires of Tr1 cells and Treg cells were cloned and expressed in the $58\alpha^-\beta^-$ T cell hybridoma cell line. The hybridomas were then co-cultured with DCs loaded with the peptides identified in the IEC MHCII peptidome. **c** Length distribution of unique peptides identified in each MHCII peptidome sample. While the Shapiro-Wilk test rejected exact normality due to the large, discrete dataset, the calculated skewness (−0.5 to 0.5) confirms that the peptide lengths (12–20 aa) lack significant skewness and exhibit an approximately normal distribution. **d** Food protein-derived peptides identified in each IEC MHCII peptidome sample. The black lines above the protein sequences indicate predicted MHCII binding sites. **e** The number of TCRs in the TCR repertoires of Tr1 cells and Treg cells that recognize food antigens presented by IECs (upper panel). The response of 6 hybridoma cell lines carrying TCRs derived from Tr1 cells to each peptide (lower panel). Hybridoma activation was assessed by NFAT-driven GFP expression. The fold change was calculated as the ratio of the percentage of GFP-positive cells in the peptide-stimulated group to that in the unstimulated baseline control. The numbers presented in the heatmap represent the mean of three replicates. n.d., not detected. **f** Representative FACS plots and quantifications of tetramer-positive Tr1 cells, Treg cells and $FOXP3^-IL\text{-}10^-$ cells sorted from the small or large intestine. Data were pooled from three independent experiments. **g–i** Tr1 or Treg cells sorted from the siLP were co-cultured with fixed IECs for 12 h. Schematic diagram of the experiment (**g**). Representative FACS plots (**h**) and quantification (**i**) of FOXP3 and IL-10 expression on sorted Tr1 or Treg cells after co-culture with IECs sorted from the indicated mice. Data were pooled from four independent experiments. **j, k** Mice were treated with tamoxifen for 5 days and Tr1 cells, Treg cells and $FOXP3^-IL\text{-}10^-$ cells were sorted and stained with Cb_{98-112} tetramer ($n = 5$). Schematic diagram of the experiment (**j**). Representative FACS plots and quantifications of tetramer-positive Tr1 cells, Treg cells and $FOXP3^-IL\text{-}10^-$ cells sorted from the siLP of mice that received the indicated treatment (**k**). Data are representative of at least three independent experiments (**a**, **e**, **f** and **g–k**). Data are mean ± SEM and were analyzed by two-tailed unpaired Student's *t*-test (**k**, right panel) and two-way ANOVA with Šídák's multiple comparisons test (**a**, **i**, and **k**, middle panel), NS, no significance; $^*P < 0.05$, $^{****}P < 0.0001$.

observed in other $TCR\alpha\beta^+$ T cell subsets within the IEL fraction, including $CD4^+CD8\alpha\alpha^+$ T cells, $CD8\alpha\beta^+$ T cells, and $CD8\alpha\alpha^+$ T cells (Supplementary Fig. S10). Remarkably, Tr1 cells in the lamina propria lymphocyte (LPL) compartment

displayed the opposite pattern, peaking at ZT14 and reaching a nadir at ZT2 (Supplementary Fig. S10). Thus, Tr1 cell dynamics in the LPL and IEL compartments follow diametrically opposed circadian rhythms.

Given the long half-life of GFP (> 24 h) , these rapid fluctuations cannot reflect *de novo* IL-10 expression. Instead, they strongly suggest physical migration of Tr1 cells between the epithelial and lamina propria compartments. Supporting this, Tr1 cells in siLP expressed genes associated with IEL adaptation (e.g., *Ccl5* and *Gzmk*; Fig. 1b). To characterize this further, we sorted total siLP CD4$^+$ T cells (FOXP3$^-$IL-10$^+$, FOXP3$^+$, and FOXP3$^-$IL-10$^-$) for single-cell RNA sequencing (Supplementary Fig. S11a). Unsupervised clustering identified eight populations. FOXP3$^-$IL-10$^+$ cells primarily occupied clusters 1 and 4, with cluster 4 displaying a canonical Tr1 signature (Supplementary Fig. S11a). Notably, cluster 4 specifically upregulated *Nkg7*, *Ccl5*, *Gzmk*, *Lag3*, *Cd7*, and *Itgae* — a gene set previously linked to CD4$^+$ T cell adaptation to the IEL niche[15,16,33].

Re-analysis of published scRNA-seq data encompassing both LPL and IEL CD4$^+$ T cells[16] confirmed that FOXP3$^-$IL-10$^+$ Tr1 cells mapped to a region bridging the LP and IEL clusters on UMAP projection (Supplementary Fig. S11b). Subcluster analysis showed FOXP3$^-$IL-10$^+$ Tr1 cells are present within both the LP and IEL T cell clusters (Supplementary Fig. S11c), and TCR repertoire analysis revealed that approximately half of the TCR clones shared between LP Tr1 cells and other subsets were shared with IEL subsets (Supplementary Fig. S11d). These data indicate a high degree of relatedness between Tr1 cells and the two IEL compartments.

Consistent with findings in the LPL, the proportion of IEL Tr1 cells was significantly reduced in AAD-fed and *H2-Ab1*$^{\Delta IEC}$ mice (Supplementary Fig. S12a, c), supporting their developmental link to LP Tr1 cells. The proportions of IL-10$^+$ T cells within other TCRαβ$^+$ T cell subsets in the IEL were largely unaffected, though total IL-10$^+$ cell numbers decreased across all populations due to reduced IEL cellularity (Supplementary Fig. S12a, c). Consistent with previous reports[15,16], we also observed an increase in the proportion of FOXP3$^+$ Treg cells and a significant decrease in the proportion of CD4$^+$CD8αα$^+$ T cells within the IEL under AAD and MHCII-deficient conditions (Supplementary Fig. S12a, c). Importantly, the circadian fluctuation of Tr1 cells in both compartments was completely absent in AAD-fed and *H2-Ab1*$^{\Delta IEC}$ mice (Supplementary Fig. S12b, d), demonstrating that IEC-mediated antigen presentation is required for these rhythmic dynamics.

The opposing circadian rhythms of Tr1 cells in the intraepithelial and lamina propria compartments, together with their IEL-adapted transcriptional signature and shared TCR clonotypes, strongly support a model in which Tr1 cells actively migrate between the epithelium and lamina propria. This dynamic shuttling provides the spatial framework necessary for Tr1 cells to receive cognate antigen directly from IECs.

Food-specific T cells were primed at mLN and developed into Tr1 cells in siLP

To investigate how food antigen-specific naïve T cells develop into Tr1 cells, we generated transgenic mice carrying the Cb4-7 TCR (Cb4-7Tg), which give the strongest response toward casein Cb_{98-112} antigen presented by IECs. Cb4-7Tg mice were crossed with IL-10^{GFP}/FOXP3^{RFP} dual reporter mice to analyze the antigen-specific Tr1 cells. Cb4-7Tg T cells could be specifically stained by the Cb_{98-112} tetramer but not OVA-specific tetramer, and the staining efficiency of Tr1, Treg and FOXP3$^-$IL-10$^-$ cells isolated from the siLP of Cb4-7Tg mice did not differ significantly (Supplementary Fig. S13a), confirming that the transgenic Cb4-7 TCR was uniformly expressed in different T cell sub-populations.

Naïve T cells isolated from Cb4-7Tg mice were transferred into recipient mice fed with CAD containing intact casein protein or AAD (Supplementary Fig. S13b). Donor cells accumulated more in the siLP of CAD-fed mice (Supplementary Fig. S13c), and approximately half acquired a FOXP3$^-$IL-10$^+$ Tr1 phenotype, whereas those in AAD-fed mice did not (Supplementary Fig. S13d, e). Since AAD feeding ablates both antigen and IEC MHCII expression[14], the requirement for cognate antigen remained unclear.

To isolate the role of cognate antigen, we transferred naïve Cb4-7Tg T cells into recipients fed either CAD or WHD that contains no casein but maintains IEC MHCII and Tr1 populations (Fig. 3a; Supplementary Fig. S13f). Donor cells acquired a Tr1 phenotype only in CAD-fed mice, and this was restricted to the siLP (Fig. 3b, c). Thus, cognate food antigen is required for Tr1 differentiation in the siLP.

Our results suggest that presentation of food antigens by IECs is critical for maintaining Tr1 cells in the small intestine (Fig. 2a). However, naïve T cells, lacking gut-homing receptors, are unable to migrate to the intestine and therefore likely have no opportunity to encounter IECs for initial activation. It was reported that oral administration of OVA generates OVA-specific T cells in the mLNs[6]. We therefore asked whether professional APCs in the mLNs initiate the response. Using *H2-Ab1* conditional knockout mice crossed to reporter strains (Supplementary Fig. S14a), we assessed Tr1 generation in the absence of MHCII on IECs (*Vil1-Cre*), DCs (*CD11c-gfp-Cre*), or B cells (*Cd19-Cre*).

In *H2-Ab1*$^{\Delta IEC}$ mice, Tr1 cells were reduced at steady state (Fig. 3d, e; Supplementary Fig. S14b), and transferred Cb4-7Tg T cells failed to become Tr1 cells (Fig. 3f, g), confirming the requirement for IEC presentation. In *H2-Ab1*$^{\Delta B}$ mice, there was no effect on Tr1 cells or donor T cell differentiation (Fig. 3d–g; Supplementary Fig. S14b), ruling out a role for B cells. In *H2-Ab1*$^{\Delta DC}$ mice, both IL-10$^+$ Treg and Tr1 cells were reduced in the siLP (Fig. 3e; Supplementary Fig. S14b). Donor Cb4-7Tg T cells showed minimal accumulation in the siLP and remained FOXP3$^-$IL-10$^-$ in *H2-Ab1*$^{\Delta DC}$ hosts (Fig. 3f, g). In the mLN, donor cells retained a naïve phenotype and failed to proliferate (Fig. 3h; Supplementary Fig. S14c, d). Thus, CD11c$^+$ DCs are essential for initial priming of food-specific T cells.

These findings suggested a two-step model: priming by DCs in mLNs, followed by IEC-driven Tr1 differentiation in the siLP. To test this, we switched AAD-fed mice to CAD and monitored Tr1 appearance. Tr1 cells emerged in the siLP after two weeks (Supplementary Fig. S14e, f). Treating mice with FTY720 (which blocks lymphocyte egress from lymph nodes) during the diet switch significantly reduced siLP Tr1 cells (Fig. 3i), indicating that recent migrants from lymph nodes were required.

We next characterized food antigen-specific T cells in the mLN. In the small intestine-draining mLN, approximately 10%

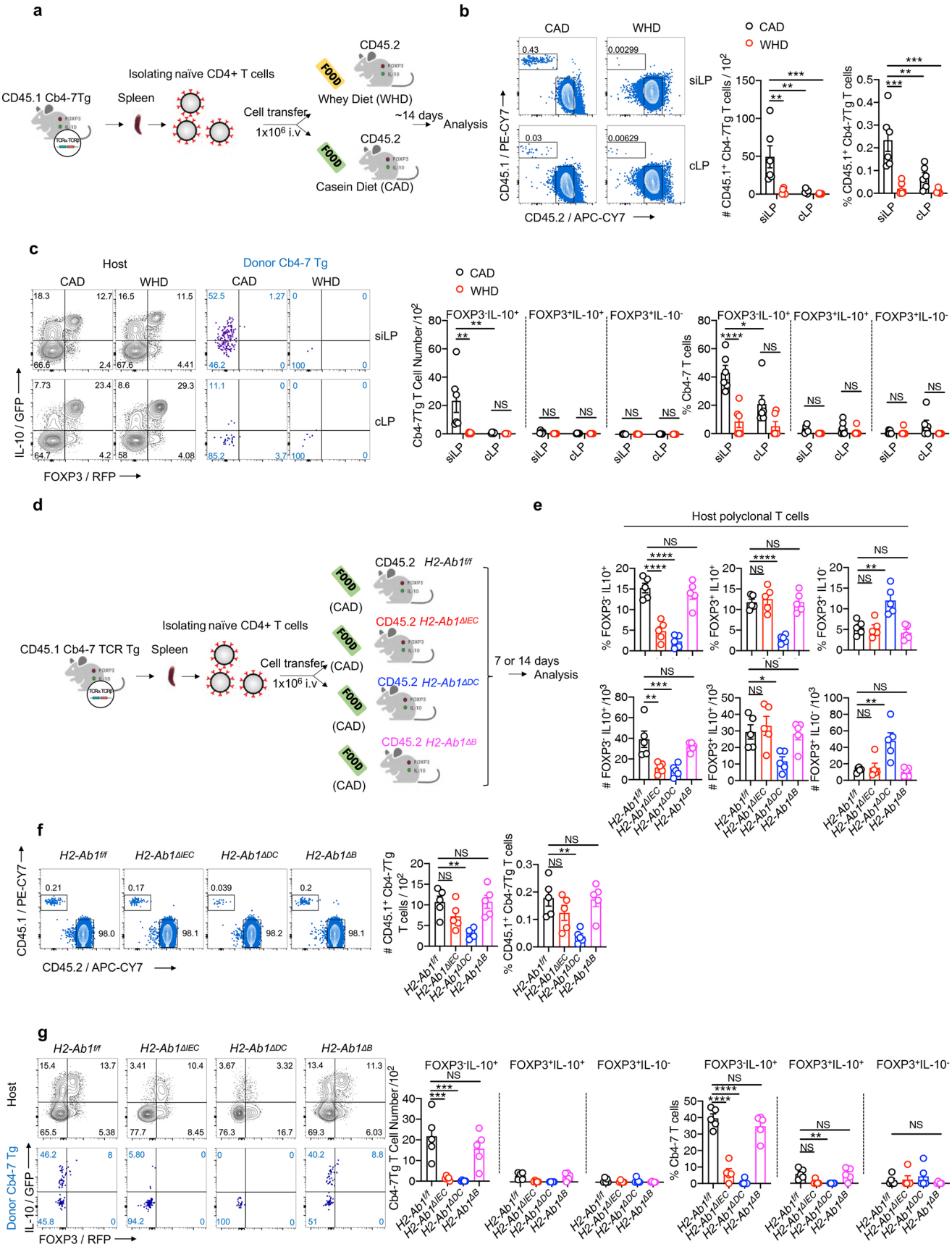
a
Isolating naïve CD4+ T cells
CD45.1 Cb4-7Tg
Spleen
Cell transfer
1x10^6 i.v
CD45.2
FOOD
Whey Diet (WHD)
~14 days
Analysis
CD45.2
FOOD
Casein Diet (CAD)
b
CAD
WHD
0.43
0.00299
0.03
0.00629
siLP
cLP
CD45.1 / PE-CY7
CD45.2 / APC-CY7
CAD
WHD
CD45.1+ Cb4-7Tg T cells / 10^2
% CD45.1+ Cb4-7Tg T cells
siLP
cLP
c
Host
Donor Cb4-7 Tg
CAD
WHD
18.3
12.7
16.5
11.5
66.6
2.4
67.6
4.41
52.5
1.27
46.2
7.73
23.4
8.6
29.3
64.7
4.2
58
4.08
11.1
85.2
3.7
siLP
cLP
IL-10 / GFP
FOXP3 / RFP
CAD
WHD
Cb4-7Tg T Cell Number /10^2
% Cb4-7 T cells
FOXP3-IL-10+
FOXP3+IL-10+
FOXP3+IL-10-
siLP
cLP
d
CD45.1 Cb4-7 TCR Tg
Spleen
Isolating naïve CD4+ T cells
Cell transfer
1x10^6 i.v
CD45.2 H2-Ab1f/f
CD45.2 H2-Ab1ΔIEC
CD45.2 H2-Ab1ΔDC
CD45.2 H2-Ab1ΔB
FOOD
(CAD)
7 or 14 days
Analysis
e
Host polyclonal T cells
% FOXP3- IL-10+
% FOXP3+ IL-10+
% FOXP3+ IL-10-
# FOXP3- IL-10+ /10^3
# FOXP3+ IL-10+ /10^3
# FOXP3+ IL-10- /10^3
H2-Ab1f/f
H2-Ab1ΔIEC
H2-Ab1ΔDC
H2-Ab1ΔB
f
H2-Ab1f/f
H2-Ab1ΔIEC
H2-Ab1ΔDC
H2-Ab1ΔB
0.21
0.17
0.039
0.2
98.0
98.1
98.2
98.1
CD45.1 / PE-CY7
CD45.2 / APC-CY7
CD45.1+ Cb4-7Tg T cells / 10^2
% CD45.1+ Cb4-7Tg T cells
g
H2-Ab1f/f
H2-Ab1ΔIEC
H2-Ab1ΔDC
H2-Ab1ΔB
Host
Donor Cb4-7 Tg
15.4
13.7
65.5
5.38
3.41
10.4
77.7
8.45
3.67
3.32
76.3
16.7
13.4
11.3
69.3
6.03
46.2
8
45.8
0
5.80
0
94.2
0
0
0
100
0
40.2
8.8
51
0
IL-10 / GFP
FOXP3 / RFP
Cb4-7Tg T Cell Number /10^2
% Cb4-7 T cells
FOXP3-IL-10+
FOXP3+IL-10+
FOXP3+IL-10-

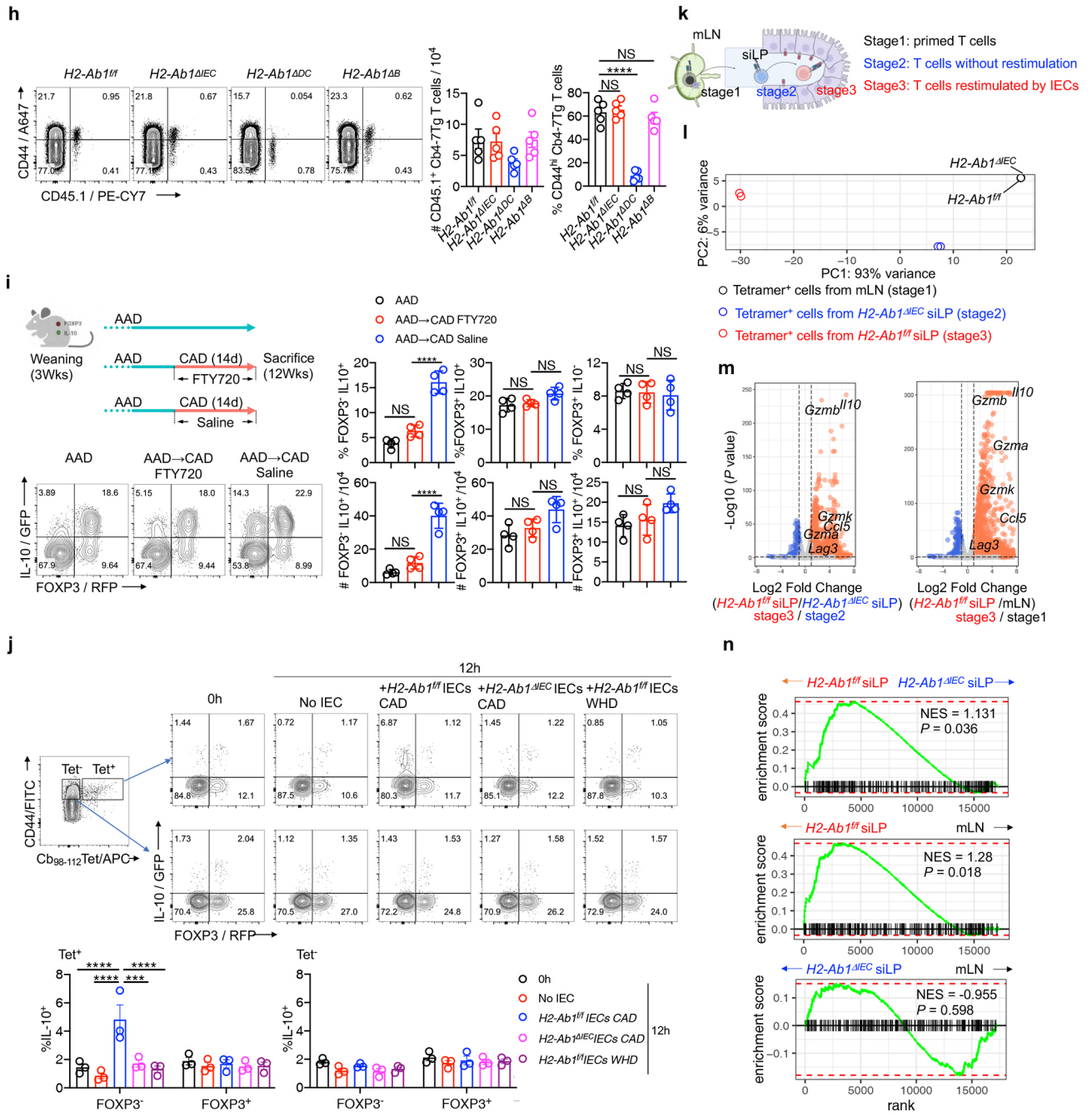

Fig. 3 Food-specific T cells were primed at gut-draining lymph node and developed into Tr1 cells in siLP. a–c Naïve CD45.1$^+$ Cb4-7 Tg T cells were transferred into CD45.2$^+$ hosts fed CAD or WHD (n = 5). **a** Experimental schematic. **b** Representative FACS plots and quantification of donor CD45.1$^+$ Cb4-7 Tg T cells in siLP or cLP of host mice. **c** Representative FACS plots and quantifications of FOXP3 and IL-10 expression in donor (CD45.1$^+$) and host polyclonal CD4$^+$ T cells from siLP or cLP. **d–h** Naïve CD45.1$^+$ Cb4-7 Tg T cells were transferred into CD45.2$^+$ *H2-Ab1*$^{\Delta IEC}$, *H2-Ab1*$^{\Delta DC}$ or *H2-Ab1*$^{\Delta B}$ hosts (n = 5). **d** Experimental schematic. **e** Quantifications of Tr1 or Treg cells in host siLP, representative FACS plots in **g**. **f** Representative FACS plots and quantifications of donor CD45.1$^+$ Cb4-7 Tg T cells in siLP of indicated hosts. **g** Representative FACS plots and quantifications of FOXP3 and IL-10 expression in donor and host CD4$^+$ T cells from siLP. **h** Representative FACS plots and quantification of CD44 expression on donor CD45.1$^+$ Cb4-7 Tg T cells in mLN. Cb4-7 Tg T cells in siLP were analyzed 14 days post-transfer; Cb4-7 Tg T cells in mLN were analyzed 7 days post-transfer. **i** Diet-switch experiment. Mice fed AAD from weaning were switched to CAD feeding 14 days before sacrifice (n = 4). Mice were injected with FTY720 (1 mg/kg/day) in saline (Top right). Representative FACS plots (lower left) and quantification (right) of FOXP3 and IL-10 expression on gated CD45$^+$CD3$^+$CD4$^+$ T cells isolated from the siLP of the indicated mice. **j** CD44^{hi}Tetramer$^+$ and CD44^{hi}Tetramer$^-$ T cells from the mLN of CAD-fed mice were co-cultured with IECs of the indicated mice for 12 h. Representative FACS plots and quantifications of FOXP3 and IL-10 expression on sorted T cells after co-culture with the indicated IECs. Data were pooled from three independent experiments. **k–n** RNA-seq analysis of CD4$^+$ T cells at stages 1–3. Stage1: casein-reactive primed T cells in mLN, CD4$^+$CD44^{hi} Cb_{98-112} tetramer$^+$ T cells from mLN of 14 *H2-Ab1*$^{f/f}$ or *H2-Ab1*$^{\Delta IEC}$ mice were pooled. Stage2: casein-reactive T cells without restimulation in siLP, CD4$^+$CD44^{hi} Cb_{98-112} tetramer$^+$ T cells from siLP of 7 *H2-Ab1*$^{\Delta IEC}$ mice were pooled. Stage3: casein-reactive T cells restimulated by IECs in siLP, CD4$^+$CD44^{hi} Cb_{98-112} tetramer$^+$ T cells from siLP of 7 *H2-Ab1*$^{f/f}$ mice were pooled. **k** Experimental schematic. **l** PCA of genome-wide gene expression of CD4$^+$ T cells at indicated stages. **m** Volcano plot of differentially expressed genes. **n** GSEA of Tr1 signature gene sets (from

GSE158703) in $CD4^+$ T cells at indicated stages. Data are representative of at least three independent experiments (**b**, **c**, **e**–**j**). Data are mean ± SEM and were analyzed by one-way ANOVA with Tukey's multiple comparisons (**e**–**h**), one-way ANOVA with Dunnett's multiple comparisons (**i**) and two-way ANOVA with Šídák's multiple comparisons test (**b**, **c**, **j**), NS, no significance; $^*P < 0.05$, $^{**}P < 0.01$, $^{***}P < 0.001$, $^{****}P < 0.0001$.

of $CD44^{hi}$ T cells stained by $Cb_{98–112}$ tetramer were Treg cells (Supplementary Fig. S14g). Less than 2% of the tetramer-positive cells were Tfh, and less than 1% of the tetramer positive Th1, Th2 or Th17 (Supplementary Fig. S14g). The other 80% tetramer-positive cells lack expression of any transcription factors or markers associated with the $CD4^+$ T cell lineages, thus being classified as Th^{lin-} cells[17] (Supplementary Fig. S14g). Food antigen-specific T cells do not acquire the Tr1 cell phenotype in mLN until they migrate into the siLP (Fig. 3g; Supplementary Fig. S14c). We therefore hypothesized that food antigen-specific T cells acquire a Tr1 cell phenotype only upon encountering food antigens presented by IECs. We sorted $CD4^+CD44^{hi}$tetramer$^+$ T cells from the small intestine-draining mLN of CAD-fed IL-10^{GFP}/$FOXP3^{RFP}$ dual reporter mice, and co-cultured these T cells with IECs isolated from the same mice. Adding IECs that present cognate dietary antigen boosted IL-10 production in the $FOXP3^-$ cell population, but not in the $FOXP3^+$ population (Fig. 3j). This effect was abrogated with MHCII-deficient IECs or IECs from WHD-fed mice (Fig. 3j). Thus, IEC presentation of cognate antigen converts mLN-primed precursors into Tr1 cells.

To define the transcriptional changes accompanying this transition, we performed bulk RNA-seq on $CD4^+CD44^{hi}$ $Cb_{98–112}$ tetramer$^+$ cells isolated from: 1. mLN of CAD-fed mice (primed precursors, stage 1); 2. siLP of CAD-fed *H2-Ab1*$^{\Delta IEC}$ mice (primed cells that migrated but lacked IEC restimulation, stage 2), and 3. siLP of *H2-Ab1*$^{f/f}$ mice (primed cells restimulated by IECs, stage 3). Cells from mLN and *H2-Ab1*$^{\Delta IEC}$ siLP exhibited similar transcriptional profiles, whereas cells from *H2-Ab1*$^{f/f}$ siLP were distinctly different (PC1 explaining 93% of variance) (Fig. 3k, l). The latter upregulated IL-10 and a core Tr1 signature (Fig. 3m, n), demonstrating that IEC restimulation drives the acquisition of the Tr1 phenotype.

Together, these data establish a new model for oral tolerance to dietary antigens: professional APCs in the mLNs prime food antigen-specific naïve T cells, generating a pool of Th^{lin-} precursors. Then the primed T cells migrate to the siLP. Upon encountering cognate antigen presented by IECs, they acquire a stable $FOXP3^-$IL-10^+ Tr1 phenotype.

Dietary antigens exhibit distinct capacities to induce Tr1 cells

Given that OVA induces antigen-specific Tregs while casein primarily induces Tr1 cells, we investigated what determines the capacity of a protein to generate Tr1 responses. Mice fed an AAD supplemented with individual dietary proteins revealed that casein and whey robustly induced siLP Tr1 cells, whereas gliadin, OVA, and peanut (PN) protein were weak Tr1 inducers (Supplementary Fig. S15a). Thus, dietary proteins differ intrinsically in their ability to drive Tr1 generation.

Since DC presentation supports both Treg and Tr1 induction, while IEC presentation selectively drives Tr1 cells (Fig. 3e; Supplementary Fig. S14b), we hypothesized that selective IEC presentation dictates Tr1-inducing capacity. To test this, mice were fed a mixed diet containing all five proteins (whey, casein, OVA, gliadin, and PN) for two weeks, and both luminal contents and IEC MHCII-bound peptides were analyzed by mass spectrometry (Supplementary Fig. S15b). While luminal peptides from all proteins were detected, only casein- and whey-derived peptides were substantially enriched among those bound to IEC MHCII (Supplementary Fig. S15c). *In silico* analysis revealed that casein- and whey-derived luminal peptides had significantly higher predicted MHCII-binding affinity than those from gliadin, OVA or PN, and the peptides presented by IECs corresponded precisely to these high-affinity sequences (Supplementary Fig. S15c). IECs lack intrinsic antigen-processing machinery and cannot present intact proteins but only pre-processed peptides (Supplementary Fig. S15d). Thus, IECs selectively present dietary proteins that generate high-affinity MHCII-binding peptides during luminal digestion.

To confirm that Tr1 cells recognize these presented epitopes, we synthesized peptides identified in the IEC MHCII immunopeptidome (2 from whey, 6 from casein, and 1 from PN) along with control peptides (2 from PN, 3 from casein, 4 from gliadin, 5 from OVA) that were absent from the peptidome despite predicted MHCII binding. Small intestinal Tr1 cells from mixed diet-fed mice responded only to the IEC-presented peptides (Supplementary Fig. S15e), validating that Tr1 cells are generated specifically in response to IEC-presented dietary epitopes.

These findings led us to hypothesize that Tr1 cells mediate tolerance to strong inducers (*e.g.*, casein, whey), while tolerance to weak inducers (*e.g.*, PN) is handled by other regulatory subsets, such as $FOXP3^+$ Tregs. To test this, we used two complementary loss-of-function models: *FOXP3*^{DTR} mice (for Treg depletion) and *H2-Ab1*$^{\Delta IEC}$ mice (which lack IEC-MHCII-dependent cells including Tr1). We first confirmed that *H2-Ab1*$^{\Delta IEC}$ mice exhibited no baseline intestinal pathology, even at 30 weeks of age, and maintained normal frequencies of all major immune cell populations, including $ROR\gamma t^+$ APCs (Supplementary Fig. S16a–f). Thus, the phenotypes observed can be attributed specifically to loss of IEC-MHCII-dependent regulation.

We then established casein and PN allergy models in these mice. Tolerized *H2-Ab1*$^{\Delta IEC}$ mice developed severe hypothermia upon casein challenge, indicating loss of tolerance (Supplementary Fig. S17a). In contrast, their response to PN challenge was only mildly affected, with the overall temperature trajectory comparable to controls (Supplementary Fig. S17b). Notably, tolerized *H2-Ab1*$^{\Delta IEC}$ mice remained significantly protected from PN allergy compared to non-tolerized controls (Supplementary Fig. S17b), suggesting that Tregs (intact in these mice) primarily maintain PN tolerance.

Conversely, in *FOXP3*^{DTR} mice, Treg depletion rendered tolerized animals highly susceptible to PN allergy, while tolerance to casein remained largely intact (Supplementary Fig. S17c, d). Even in the absence of Tregs, casein-challenged mice remained significantly protected compared to non-tolerized controls (Supplementary Fig. S17c), confirming that Tr1 cells

are sufficient to maintain casein tolerance independently of Tregs.

Together, these complementary genetic models reveal a clear division of labor among regulatory T cell subsets: Tr1 cells — induced by IEC presentation of high-affinity dietary peptides — are essential for tolerance to strong inducers like casein; while FOXP3$^+$ Tregs are essential for tolerance to weak inducers like PN, which fail to engage the IEC–Tr1 pathway. This functional specialization ensures that the intestinal immune system can mount appropriate regulatory responses to the diverse array of dietary antigens encountered.

Targeted delivery of synthetic peptides from PN allergens to IECs induces PN-specific Tr1 cells and protects mice from PN allergy.

PN is a common food allergen and, unlike casein or whey, a weak Tr1 inducer (Supplementary Fig. S15a). We asked whether enforced presentation by IECs of synthetic PN epitopes — which are absent from the intestinal lumen under physiological conditions — could generate PN-specific Tr1 cells and confer protection. To achieve epithelium-specific delivery, we employed a positively glucosylated nanoparticle (PGNP) system that targets small intestinal epithelial cells via glucose transporters[34].

Gavaging mice with PGNPs loaded with FITC-labeled casein peptides resulted in peak fluorescence in the proximal small intestine at 1 h, declining by 4 h and returning to baseline by 8 h (Supplementary Fig. S18a). Compared to free peptides, PGNP encapsulation markedly improved intestinal delivery efficiency and prevented accumulation in the large intestine (Supplementary Fig. S18a). Crucially, because the targeted glucose transporters are expressed exclusively on epithelial cells (Supplementary Fig. S18b), PGNP delivery avoided uptake by CD11c$^+$ APCs (Supplementary Fig. S18c).

To test whether PGNP-delivered peptides are presented by IECs, we gavaged WHD-fed mice (no dietary casein source) with PGNPs loaded with a cocktail of eight casein epitopes (PGNPs-CASB) identified in the IEC MHCII immunopeptidome (Figs. 2e, 4a). IECs were isolated 1 h later and co-cultured with Tr1 cells from CAD-fed mice. Only IECs from PGNPs-CASB-treated mice sustained IL-10 expression by Tr1 cells; IECs from mice given empty PGNPs, free casein peptides, or PGNPs-OVA$_{323\text{-}339}$ were ineffective (Fig. 4a, b). The stimulatory capacity of IECs peaked at 1 h post-gavage and declined thereafter, mirroring PGNP absorption kinetics (Supplementary Fig. S18d).

We next applied this approach to PN. Eight synthetic peptides derived from Ara h 1, h 2, and h 3 — predicted to bind MHCII but not generated during luminal digestion (Supplementary Fig. S15c) — were encapsulated in PGNPs (PGNPs-PN). These peptides were potential T cell epitopes and confirmed to bind MHCII (Supplementary Fig. S19a–c). Mice were gavaged daily with PGNPs-PN or controls for one week, after which siLP Tr1 cells were isolated and co-cultured with peptide-pulsed DCs (Fig. 4c). Only Tr1 cells from PGNPs-PN-treated mice produced IL-10 upon restimulation (Fig. 4d; Supplementary Fig. S18e), demonstrating successful induction of PN-specific Tr1 cells.

To assess therapeutic efficacy, we used the BALB/c mouse strain, which mounts robust Th2 responses to sensitization. PGNPs delivery efficiency was equivalent between C57BL/6 and BALB/c mice (Supplementary Fig. S20a). Because IL-10/FOXP3 reporters are not available on the BALB/c background, we identified CD25^{lo}LAG3$^+$ as a surface marker combination that selectively enriches for Tr1 cells in the siLP (Supplementary Fig. S21a–c). Consistent with findings in C57BL/6 mice, BALB/c IECs did not naturally present PN peptides after feeding intact PN protein, but efficiently presented PGNP-delivered peptides, leading to the generation of PN-specific CD25^{lo}LAG3$^+$ IL-10$^+$ Tr1 cells (Supplementary Fig. S20b–h, Tables S3, S4).

PN-sensitized BALB/c mice were treated for three weeks with PGNPs-PN, empty PGNPs, or free PN peptides, then challenged with PN extract (Fig. 4e). PGNPs-PN-treated mice exhibited significantly reduced hypothermia (Fig. 4f), lower serum PN-specific IgE and IgG (Fig. 4g, h), and reduced mMCP-1 levels, a hallmark of anaphylaxis (Fig. 4i). Thus, targeted delivery of synthetic PN peptides to IECs induces protective Tr1 cells and ameliorates PN allergy (Fig. 4j).

These findings establish that the IEC-Tr1 axis can be therapeutically harnessed to induce antigen-specific tolerance even for allergens that naturally evade this pathway. By bypassing the constraints of luminal digestion, PGNP-mediated peptide delivery offers a novel and translatable strategy for food allergy immunotherapy.

DISCUSSION

Although Tr1 cells have been implicated in various immune-mediated pathologies, their physiological role in responding to specific antigens has remained unclear[30]. Here, we demonstrate that siLP Tr1 cells recognize food antigens presented by IECs and actively maintain immune tolerance to dietary proteins.

Mice and humans harbor two major regulatory CD4$^+$ T cell subsets — Tr1 and Treg — with distinct transcriptional programs. Unlike Tregs, which follow a well-defined developmental pathway, Tr1 cells are highly plastic: they can arise from memory T cells or transdifferentiate from Th1, Th2, and Th17 effectors[29,30]. Our data support this view. *In vitro*, Tregs maintained stable IL-10 expression, whereas Tr1 cells rapidly lost IL-10 unless co-cultured with antigen-presenting IECs. We propose that this plasticity is shaped by the host's feeding cycle: IL-10 production by Tr1 cells is conditionally induced only when dietary antigens are actively presented by IECs, ensuring that tolerance is maintained specifically during nutrient intake.

Different dietary antigens elicit distinct CD4$^+$ T cell responses. Oral administration of a *Toxoplasma* peptide induces Th^{lin-} cells in mLNs[17], while ovalbumin favors Treg induction[6,19]. Our data reveal that dietary proteins vary markedly in their Tr1-inducing capacity: casein and whey drive robust Tr1 expansion, whereas PN, gliadin, and OVA are poor inducers. Using complementary loss-of-function models, we show that tolerance to strong Tr1 inducers is primarily mediated by Tr1 cells, whereas tolerance to weak inducers is governed by Tregs. This division of labor extends previous work demonstrating the importance of dietary antigens for small intestinal Treg maintenance[20]. We acknowledge that our use of the *H2-Ab1*$^{\Delta IEC}$ model cannot fully exclude contributions from other food-reactive T cells (*e.g.*, CD4$^+$CD8αα$^+$

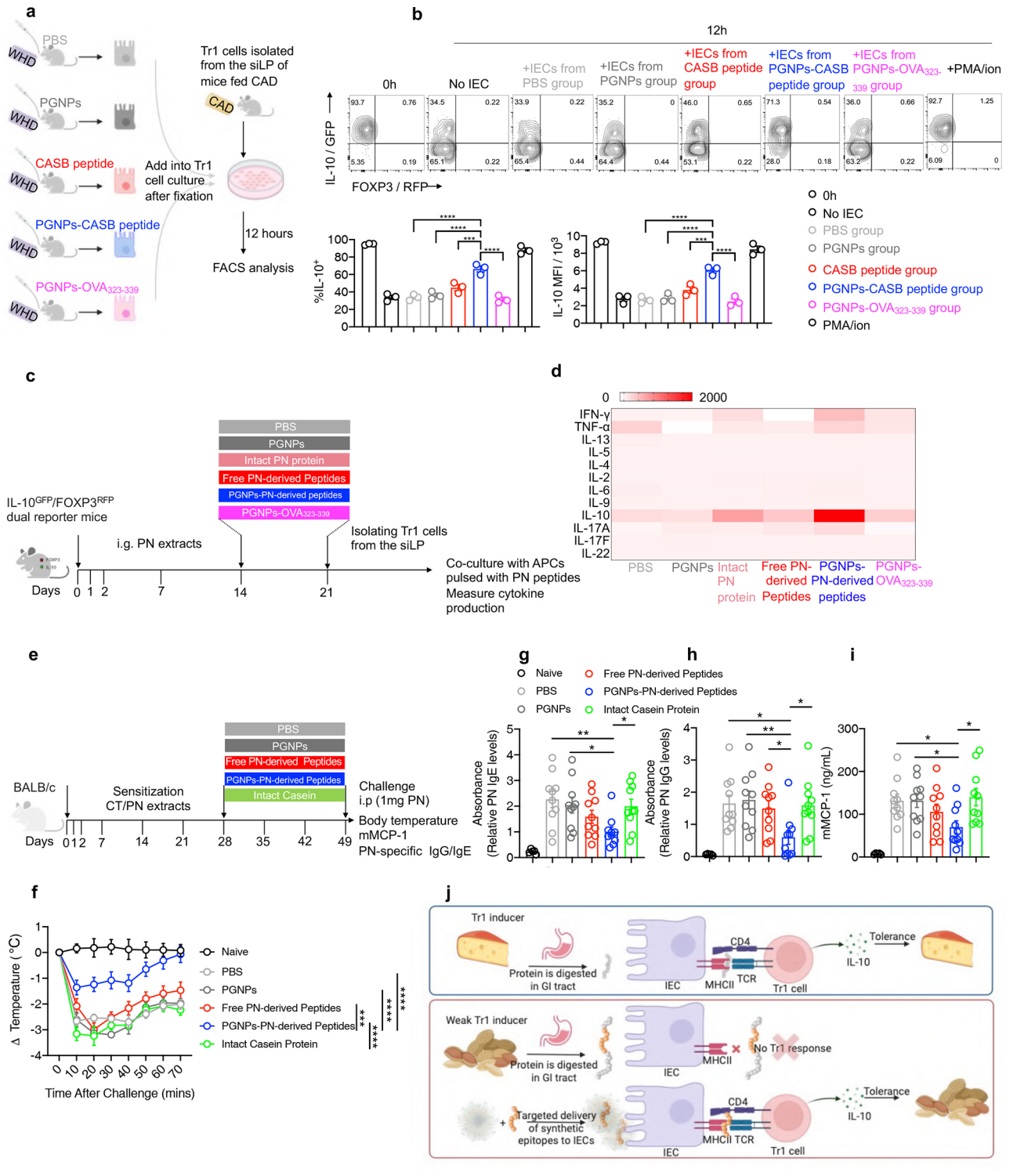

Fig. 4 Targeted delivery of synthetic peptides from PN allergens to IECs induces PN-specific Tr1 cells and protects mice from PN allergy. a, **b** Tr1 cells sorted from the siLP of CAD-fed mice were co-cultured with fixed IECs sorted from WHD-fed mice receiving the indicated treatments for 12 h. Mice were orally gavaged at ZT0 with PGNPs loaded with 0.2 mg of peptides, using an equal amount of free peptides as a control. Experimental scheme (**a**). Representative FACS plots and quantification of FOXP3 and IL-10 expression in siLP Tr1 cells post-co-culture with IECs from the indicated mice (**b**). Data were pooled from three independent experiments. **c**, **d** Mice received the indicated daily oral gavage treatments for 1 week post-PN exposure. Mice were orally gavaged with a total of 0.4 mg of PGNPs-loaded peptides administered across two time points daily (ZT0 and ZT12). Experimental scheme (**c**). siLP Tr1 cells were isolated and co-cultured with peptide-pulsed DCs (**d**). After 24 h, culture supernatants were collected for cytokine analysis. Tr1 cells were pooled from 2–3 mice. The heatmap displays the mean of three replicates, and the raw data are presented in Supplementary Fig. S18e. **e**–**i** PN allergy model: BALB/c mice were sensitized 7 times with PN extract plus cholera toxin on the indicated schedule, followed by twice-daily oral gavage (at ZT0 and ZT12) of a total of 0.4 mg of PGNPs-loaded peptides for 3 weeks, starting at day 28 before the final allergen challenge (n = 10 mice per group). Change in core body temperature (**f**), serum mMCP-1 (**g**), and PN-specific IgE (**h**) and IgG (**i**) in serum collected 80 min or 24 h post-challenge were measured.

j Schematic diagram showing the experimental rationale. Unlike Tr1 inducers whose proteins can be degraded into MHCII-binding peptides in the gut lumen, weak Tr1 inducers cannot generate MHCII-binding epitopes for IEC presentation. Targeted delivery of weak inducer epitopes to IECs may artificially induce specific Tr1 cells. Data are representative of at least three independent experiments. Data are mean ± SEM and were analyzed by two-way RM ANOVA (**f**) and one-way ANOVA with Tukey's multiple comparisons (**b, g–i**). NS, no significance; $^{*}P < 0.05$, $^{**}P < 0.01$, $^{***}P < 0.001$, $^{****}P < 0.0001$.

IELs)[15]; cleaner Tr1-specific loss-of-function models will be required in future studies. A key obstacle to developing such models is that a specific transcription factor for intestinal Tr1 cells has not yet been identified; although these cells have been shown to express T-bet[27], the broad expression of T-bet across multiple $CD4^+$ T cell subsets makes it unsuitable as a definitive Tr1 marker.

Previous studies established that IEC MHCII is required for generating food-reactive $CD4^+CD8\alpha\alpha^+$ IELs[15,16,21] and for preventing food allergy[14]. Here, we provide direct molecular evidence: mass spectrometry identified casein-derived peptides bound to IEC MHCII, and we isolated Tr1 TCRs that specifically recognize these IEC-presented epitopes. Thus, IEC-expressed MHCII directly participates in mediating food tolerance.

IECs cover the entire intestinal mucosa and consequently present vast amounts of antigen. Previous studies demonstrate that Tr1 cell generation depends on cognate antigen dose, with high concentrations of MHCII-restricted antigens promoting Tr1 cell development[24]. When food antigen-specific T cells migrate to the small intestine, they encounter abundant food antigens presented by IECs — this likely explains why IECs specifically induce Tr1 cell differentiation in the small intestine[14].

IECs present food antigens that have been pre-processed in the intestinal lumen during absorption. Compared to tolerance induction by professional APCs — which require uptake, processing, and migration[1] — IEC-driven tolerance may be more rapid and efficient. This efficiency likely explains why Tr1 cells, which depend on continuous antigen encounter, are preferentially maintained in the siLP.

Notably, Tr1 cells are virtually absent from mLNs; food-specific cells are predominantly Th^{lin-}, consistent with prior reports[17]. Thus, mLN-primed precursors do not differentiate into Tr1 cells until they migrate to the intestine and re-encounter antigen on IECs. Our FTY720 experiments (Fig. 3i) support this two-step model but do not establish direct temporal causation. Definitive proof will require temporal fate-mapping studies to track mLN-primed cells as they migrate and convert into mature Tr1 cells in the siLP. Such a fate-mapping system would, in addition, help address whether food antigen-specific Tr1 cells can originate from other effector T cell subsets through transdifferentiation, given previous reports that Th1 and Th17 cells are capable of converting into Tr1 cells[30].

APCs within the mLN exhibit a distinct functional division of labor, with recent studies identifying a specialized population of $ROR\gamma t^+$ APCs (tolerogenic DCs, Thetis cells) that drive food-specific Treg induction[6–9]. Our two-step model indicates that Tr1 precursors are also primed by $CD11c^+$ APCs in the mLN. However, because we used a generalized *CD11c-gfp-Cre* model, we cannot pinpoint the exact APC subset responsible. It is possible that distinct APC subsets in the mLN produce different signal 2 or signal 3 and preferentially present different types of luminal antigens, such that tolerance to different antigen sources is mediated by distinct regulatory T cell populations. For example, $ROR\gamma t^+$ APCs may process latent TGF-β through αvβ3 integrin expression to maintain $ROR\gamma t^+$ Tregs[35], whereas cDC1s may endow precursors with Tr1 differentiation potential through IL-27 secretion[36]. Future studies using lineage-specific APC loss-of-function models and fate-mapping of Th^{lin-} precursors will be necessary to resolve this question.

Recent clinical trials have demonstrated that oral immunotherapy (OIT) can induce desensitization and sustained unresponsiveness in both children[37] and adults[38] with food allergies. OIT engages tolerogenic pathways, including the induction of allergen-specific Tregs. Our study offers a complementary approach: PGNP-mediated delivery of synthetic PN peptides to IECs induces PN-specific Tr1 cells and mitigates anaphylaxis in allergic mice.

Unlike conventional OIT using intact allergens, our strategy uses defined peptide epitopes that are intrinsically less immunogenic and targeted specifically to IECs, minimizing uptake by professional APCs and reducing the risk of IgE cross-linking and subsequent degranulation of mast cells and basophils. This may offer an improved safety profile for oral immunotherapy. Genetic confirmation that this tolerance depends on IEC antigen presentation would further strengthen the mechanistic basis and help anticipate potential off-target effects.

PGNP-PN peptide treatment conferred significant but incomplete protection, suggesting that Tr1 cells alone are insufficient for full tolerance. Conventional OIT with intact PN protein, while ineffective at inducing Tr1 cells, robustly engages the Treg compartment. We therefore propose that a combination strategy — conventional OIT to induce Tregs together with targeted PGNP-peptide delivery to induce Tr1 cells — could harness both regulatory networks synergistically for enhanced therapeutic benefit. Understanding whether IECs exhibit preferential presentation of certain delivered peptides would further inform peptide selection and optimize the tolerogenic capacity of this approach.

MATERIALS AND METHODS

Mice

$IL\text{-}10^{GFP}/FOXP3^{RFP}$ dual reporter mice ($IL\text{-}10^{GFP/+}$ mice crossed with $FOXP3^{RFP}$ mice) and CD45.1 mice were kindly provided by Prof. Richard A. Flavell of Yale university school of medicine. *Vil1-Cre*, *CD11c-gfp-Cre* mice were provided by Dr. Rongbin Zhou of University of Science and Technology of China (USTC). *Cd19-Cre* mice were purchased from GemPharmatech (Nanjing, CN). Cb4-7 TCR transgenic mice were generated in our lab. $Vil1^{CreERT2}$ mice were provided by Dr. Wen Pan of USTC. Sex- and age-matched littermates aged of 8–10 weeks were used in most of the studies except for those in

diet switch experiment (Sacrificed at 12 weeks old) or those fed AAD (weaning). All mice were kept under specific pathogen-free (SPF) conditions under a strict 12-h light cycle (lights on at 08:00 and off at 20:00) in the animal facility at USTC. All experimental procedures carried out in mice were with reference to the National Guidelines for Animal Usage in Research (China) and were approved by the Animal Ethics Committee of USTC (USTCACUC212101033).

Diet

The AAD was customized by Trophic diet (Jiangsu, CN). The ingredients of AAD were listed as follows (g/kg): L-Alanine 4.5; L-Arginine, 6.3; L-Aspartic Acid 11.3; L-Cystine 3.7; L-Glutamic Acid 36.2; Glycine 3.1; L-Histidine, 4.5; L-Isoleucine 8.4; L-Leucine 15.3; L-Lysine-HCl 16.1; L-Methionine 4.5; L-Phenylalanine 8.7; L-Proline 20.4; L-Serine 9.4; L-Threonine 6.6; L-Tryptophan 2.1; L-Tyrosine 9.2; L-Valine 9.9; Sucrose 100; Cornstarch 399.886; Dyetrose 145; Soybean Oil 70; tBHQ 0.014; Cellulose 50; Salt Mix 35; Sodium Bicarbonate 7.4; Vitamin Mix 10; Choline Bitartrate 2.5. In the second week after birth, the diet in the breeding cages was replaced with AAD, and after weaning, the mice were fed AAD until they were sacrificed. Casein diet and whey diet are also purified diets that purchased from Trophic diet (Jiangsu, CN). The composition of these diets is identical to AAD, except that the amino acids are replaced by an equivalent amount of intact proteins. All diets were irradiated, vacuum-packed and stored at −20 °C. The diets placed in the mouse cages were changed twice a week. All mice had *ad libitum* access to food.

Antibodies, flow cytometry and cell sorting

Single-cell suspensions were incubated on ice with conjugated antibodies in MACS buffer (PBS containing 2% FBS and 1 mM EDTA). Unlabelled anti-CD16/32 (clone 93, Biolegend) was used to block Fc receptors. Dead cells were excluded with Zombie Aqua™ dye (Biolegend) or DAPI (3 μM, Biolegend). The following antibodies were used for mouse cell-surface staining: CD4 PE/Cy7 (GK1.5) Biolegend 100422, CD45 PerCP/Cy5.5 (30-F11) Biolegend 103132, CD4 PerCP/Cy5.5 (GK1.5) Biolegend 100434, CD45.1 PE/Cy7 (A20) Biolegend 110730, CD45.2 PE/Cy7 (104) Biolegend 109830, CD3 APC/Cy7 (17A2) Biolegend 100222, CD4 APC (GK1.5) Biolegend 100412, CD49b APC (HMα2) Biolegend 103516, LAG-3 PE/Cy7 (C9B7W) Biolegend 125226, CD90.1 PE (OX-7) Biolegend 202524, TCRβ APC (H57-597) Biolegend 109212, CD3 PE/Cy7 (17A2) Biolegend 100220, CD4 Super Bright 600 (RM4-5) Invitrogen 63-0042-82, CD45.2 APC/Cy7 (104) Biolegend 109824, I-A/I-E FITC (M5/114.15.2) Biolegend 107606, CD326 (EpCAM) APC (G8.8) eBioscience 17-5791-82, CD11c PE (N418) Biolegend 117308, CD11c PerCP/Cy5.5 (N418) Biolegend 117328, CD19 APC/Cy7 (6D5) Biolegend 115530, CD170 (Siglec-F) APC (S17007L) Biolegend 155507, CD11b RY610 (M1/70) BD 758338, TCRβ Alexa Fluor 700 (H57-597) Biolegend 109224, CD19 BV605 (6D5) Biolegend 115540, F4/80 BV421 (T45-2342) BD 565411, Ly6C PerCP/Cy5.5 (HK1.4) Biolegend 128012, XCR1 BV650 (ZET) Biolegend 148220, CD117 (c-kit) APC (2B8) Biolegend 105812, FcεRIα FITC (MAR-1) Biolegend 134306, CXCR5 PE (L138D7) Biolegend 145504, I-A/I-E APC/Cy7 (M5/114.15.2) Biolegend 107628, CD45.2 APC (104) Biolegend 109814, CD44 FITC (IM7) Biolegend 103006, CD44 Alexa Fluor 647 (IM7) Biolegend 103018, CXCR5 PE/Cy7 (L138D7) Biolegend 145516, TCRβ BV650 (H57-597) Biolegend 109251, CD25 APC (PC61) Biolegend 102012. Except for CD49b and LAG-3, which were stained at 37 °C for 30 min, all other surface markers were stained at 4 °C for 15 min. The following antibodies were used for mouse intracellular staining: Tbet PE/Dazzle™ 594 (4B10) Biolegend 100456, GATA3 PE (L50-823) BD 560068, RORγt BV650 (Q31-378) BD 564722, RORγt PE (AFKJS-9) Invitrogen 12-6988-82, GATA3 BV421 (L50-823) BD 563349, FOXP3 Alexa Fluor 647 (MF-14) Biolegend 126408, IFN-γ PE/Cy7 (XMG1.2) Biolegend 505826, IL-17A APC (TC11-18H10.1) Biolegend 506916, IL-4 PE (11B11) Biolegend 504104.

For intracellular transcription factor staining, cells were fixed/permeabilized for 30 min at room temperature or overnight at 4 °C with FOXP3/Transcription Factor Staining Buffer Set (eBioscience). Then the cells were washed with 1× Permeabilization solution (eBioscience) and stained with fluorescently-conjugated antibodies in 1× permeabilization buffer for 30 min at room temperature. Stained cells were washed three times with 1× PBS. For intracellular cytokine staining, cells were first incubated for 4 h in RPMI 1640 medium with 10% FBS, Cell Stimulation Cocktail (Invitrogen) at 37 °C. Then cells were fixed/permeabilized for 20 min at 4 °C with Fixation/Permeabilization Solution Kit (BD) and then washed with 1× Permeabilization solution (BD) and stained with fluorescently-conjugated antibodies in 1× permeabilization buffer for 30 min at 4 °C. Stained cells were washed three times with 1× PBS. Flow cytometry data were collected using CytoFlex S (Beckman Coulter) or Cytek Aurora (Cytek) and analysed with FlowJo V10 software (Tree Star). Lymphocytes were sorted using FACSAria Fusion (BD) or CytoFlex SRT (Beckman Coulter). IECs were sorted by CytoFlex SRT using vertical sorting mode.

For analysis of cell numbers, the number of cells per microliter was obtained from the Cytoflex S. This number was first multiplied by 200 to obtain the total number of cells per tube and then multiplied by 5 to obtain the total number of cells in the intestinal segment, since only one fifth of the cells were stained for flow cytometry analysis. For the small intestine, the total number of cells in the whole small intestine was multiplied by 4 based on the total number of cells in the intestinal segment, since only one quarter of the tissue was taken for digestion due to the length of the small intestine (one quarter each of the duodenum, jejunum, and ileum).

Cell isolation from the intestine

Mice were lethally anesthetized with pentobarbital sodium and perfused with PBS containing 2.5% FCS. For the isolation of IECs and intraepithelial lymphocytes, intestinal tissues were excised and flushed thoroughly with ice-cold PBS. Use ophthalmic forceps to remove the fat tissue on the surface of the intestine under a stereomicroscope. The intestines were then turned inside out and cut into 1 cm sections then transferred into RPMI with 1.5 mM EDTA (Sigma-Aldrich) and 2% FCS, and shaken for 15 min at 37 °C. Supernatants were collected through a 100-μm cell strainer to get single-cell suspensions containing both epithelial cells (~90%) and lymphocytes (IEL, ~10%).

For the isolation of lamina propria lymphocytes, intestinal

tissues were excised and flushed thoroughly with ice-cold PBS. Ophthalmic forceps were used to remove the fat tissue on the surface of the intestine under a stereomicroscope. The intestines were then turned inside out and cut into 1 cm sections then transferred into RPMI with 1.5 mM EDTA, 1mM dithiothreitol (Sigma-Aldrich) and 2% FCS, and shaken for 15 min at 37 °C for 3 times. Then the supernatants were discarded. Tissue sections were collected and washed with RPMI with 3% FCS (EDTA-free) for another 5 min. The intestinal sections were transferred into digestion buffer (RPMI with 0.5 mg/mL collagenase II (Sigma-Aldrich), 0.5 mg/mL Dnase I (Roche) and 5% FBS (Gibco)) and shaken for 35 min at 37 °C. The digestion was stopped by adding EDTA to the digestion buffer. Supernatants were collected through a 100-µm cell strainer to get single-cell suspensions and lymphocytes were enriched by 40% Percoll (Cytiva) gradient centrifugation.

Tissue digestion

Mice were lethally anesthetized with pentobarbital sodium and perfused with PBS containing 2.5% FCS. Tissues were harvested into HBSS with 2.5% FCS and 2 mM EDTA, and stored on ice until further processing. The thymus, lymph nodes, Peyer's patches, spleen, and adrenal glands were dispersed onto frosted glass microscope slides, and filtered through 100 µm mesh. Where necessary, erythrocytes were lysed prior to counting using a Countess Automated Cell Counter (ThermoFisher Scientific). The liver was prepared similarly, except the resulting cell suspension was washed extensively and centrifuged (600× *g*, 10min) through a 40% Percoll (Sigma Aldrich) solution prior to erythrocyte lysis. Bone marrow was extracted from a single femur by crushing with a mortar and pestle. Blood was treated to lyse red cells prior to staining.

The salivary glands, lungs, pancreas, kidney, adipose tissue, reproductive tissues, eyes, back skin, tongue, hind limb muscle, heart, bladder and brain were digested as follows to extract tissue leukocytes: tissues were chopped finely with razor blades and washed by centrifugation to remove debris. They were then resuspended in digest buffer (IMDM supplemented with 20% FCS, 10 mM HEPES, 1 mM sodium pyruvate, 10 µg/mL gentamicin, 1mM $CaCl_2$ and 1mM $MgCl_2$) with enzymes (400 µg/mL collagenase IV, 100 µg/mL hyaluronidase and 40 µg/mL DNase I, Sigma Aldrich). Tissues were shaken in an agitating mixer at 37 °C for 15 min, dispersed with a pipette, and shaken for another 15 min. The solution was then filtered through 100 µm mesh and any remaining chunks were forced through the mesh. The cells were washed and passed through 40% Percoll to enrich for the leukocyte fraction.

Single cell RNA and TCR sequencing

We used hashtag reagents for sample barcoding, enabling the amalgamation of two samples into a single lane for subsequent demultiplexing during analysis. Specifically, the hashtags consisted of two antibodies recognizing ubiquitous surface markers, CD45 and MHC class I, each conjugated to the same oligonucleotide containing the barcode sequence.

Lamina propria lymphocytes were isolated from the proximal small intestine of IL-10^{GFP}/$FOXP3^{RFP}$ dual reporter mice and Tr1 and Treg cells were sorted. Cell viability and integrity were evaluated by Trypan blue staining. Subsequently, cells were incubated with 1 µL (0.5 µg) of the respective Totalseq-C (Hashtag1 for Tr1 cells and Hashtag2 for Treg cells) anti-mouse Hashtag antibodies (155861 and 155863, BioLegend) for 30 min at 4 °C. After staining, the samples were washed twice with 500 µL of cell staining buffer (BioLegend) and pooled into a single tube. The ratio of Tr1 and Treg cells was not adjusted. Finally, the cells were re-suspended in a resuspension buffer (PBS containing 0.04% BSA). The cell number and viability were evaluated again, and the optimal cell concentration (700–1200 cells/µL) was set according to the 10X Genomics protocol.

Cells were loaded onto the 10X Chromium Single Cell Platform (10X Genomics) at a concentration of 1,000 cells per µL (Single Cell 5' library and Gel Bead Kit v.2) as described in the manufacturer's protocol. Generation of gel beads in emulsion (GEMs), barcoding, GEM-RT clean-up, complementary DNA amplification, gene and TCR, and hashtag library construction were all performed as per the manufacturer's protocol. Qubit was used for library quantification before pooling. The final library pool was sequenced on the Illumina Novaseq 6000 instrument using 150-base-pair paired-end reads.

Gene expression count matrices were generated using Cell Ranger version 5.0 count method using the default parameters. Sequencing files were aligned to the refdata-gex-mm10-2020-A reference library provided by 10X Genomics. Raw outputs from Cell Ranger were processed in the Seurat R package (4.1.1). hashing-based doublet detection strategy HTODemux was used to identify doublets that represent two or more cells from different samples (positive.quantile = 0.99). Genes whose sum of expression in all cells was less than 3 were deleted. We retained cells that had unique feature counts within the range of 200 to 5,000 and mitochondrial counts of less than 10%, log-normalized the counts and scaled each gene. 2,000 highly variable features were determined using the "vst" method (FindVariableFeatures function), and served as input to the principal component analysis for dimensionality reduction. We used the first 25 principal components to cluster cells using the Louvain algorithm. To determine cluster-specific transcriptional programs, differential gene expression analysis was performed with Wilcoxon Rank Sum Test.

Single-cell TCR sequencing data were assembled and the clonotypes were determined using the default settings of Cell Ranger version 5.0 VDJ pipeline. CombineTCR and combineExpression function in scRepertoire (2.0.0) package was used to merge scTCR-seq data with the Seurat object of scRNA-seq data. The relative number of clonotypes shared between each cell type was calculated using the getCirclize function. The Circos plot was generated by R package circlize (0.4.16).

IEC MHCII peptidome

Epithelial cells from the proximal small intestine of the same mice that underwent single-cell RNA and TCR sequencing were used for MHCII-associated peptide isolation. IECs were sorted by CytoFlex SRT using vertical sorting mode. A minimum of 1×10^7 IECs was used per immunoprecipitation. Cells were lysed and homogenized in immunoprecipitation buffer (YUBiomics) under protease-inhibiting conditions to preserve

native peptide–MHC complexes. MHCII–antigen complexes were enriched using an anti-mouse MHC class II (I-A/I-E) antibody (clone M5/114.15.2, BioXcell) crosslinked to Protein G Magnetic Beads (Promega), according to the YUBiomics NeoAntigen Platform protocol. Prior to large-scale immunoprecipitation, SDS-PAGE analysis confirmed reproducible antibody crosslinking efficiency. Following capture, extensive washing steps — including detergent removal, high-salt washes, and PBS washes — were performed to eliminate non-specifically bound proteins.

Bound MHCII-peptide complexes were eluted, and peptides were dissociated by treatment with 10% acetic acid. To monitor recovery quality, western blot analysis of the second elution fraction was performed to confirm the presence of MHCII molecules as an internal control for successful immunoprecipitation. Peptides were then separated from MHCII molecules by centrifugal filtration through 10-kDa molecular weight cutoff filters. The peptide-containing flow-through was desalted using C18 spin columns. Peptide solubility was subsequently verified, and samples were filtered to prevent LC column blockage. The final eluates were lyophilized (dried) and stored at −80 °C prior to mass spectrometry analysis.

Mass spectrometric analysis was performed using a timsTOF Pro mass spectrometer (Bruker Daltonics) coupled to an Evosep One liquid chromatography system (Evosep). Peptides were separated using a 21-min gradient method. The mass spectrometer was operated in data-dependent acquisition mode with the following parameters: MS1 scan range of 100–1,700 m/z in positive ion mode; accumulation and ramp times of 100 ms each; dynamic exclusion duration of 24 sec; ion source voltage set to 1,500 V; source temperature maintained at 180 °C; and dry gas flow rate of 3 L/min. Ion mobility separation was conducted with a mobility range of 0.75–1.35 Vs/cm2, followed by the acquisition of 8 PASEF MS/MS scans per cycle.

The acquired raw data were processed using PEAKS X Pro software (version 10.6, Bioinformatics Solutions Inc.). The data were searched following stringent criteria: High-confidence peptides: Peptide-spectrum match (PSM) FDR < 0.1%; Medium-confidence peptides: FDR < 0.5%. For peptide identification, we integrated the host proteome with several specialized databases, including proteomes of species identified by metagenomic sequencing of proximal small intestinal contents and tissue, and proteomes of species detected in the enzymatically digested GBD via mass spectrometry.

To ensure technical consistency and establish quality control benchmarks, pilot experiments were conducted using A20 cells. For 1×10^8 A20 cells, consistent recovery of > 4,500 unique 12–20mer peptides at a 1% false discovery rate (FDR) is expected, with a predominant length distribution of 16-mers (> 50%). Peptide identification reproducibility across biological and technical replicates was further validated by motif clustering analysis using GibbsCluster, which demonstrated consistent clustering of canonical H2-IAb binding motifs. Finally, biological reproducibility was confirmed by performing an independent replicate experiment for the IEC-MHCII immunopeptidome in Fig. 2d, which successfully identified the identical casein epitopes presented by IECs, strictly consistent with our initial findings (peptides identified in the independent replicate experiment were listed in Supplementary Table S5). A complete list of all identified peptides, including spectral counts, FDR values, and sequence information, is provided in Supplementary Tables.

Bulk RNA sequencing

Total RNA was extracted from T cells by using TRIzol reagent (TIANGEN) according to the manufacturer's instructions. RNA-seq libraries were sequenced using the 100-bp paired-end mode via the DNBseq (BGI) according to the manufacturer's protocol. The raw reads were filtered by removing adaptor sequences, contamination, and low-quality reads. Cleaned reads (20 million reads per sample) were aligned to the mm10 reference genome using STAR (Version 2.7.1). The quantification results from 'featureCount' were then analyzed with the Bioconductor package DESeq2 (1.32.0), which fits a negative binomial distribution to estimate technical and biological variability. PCA plot was generated to identify sample outlier. Differentially expressed genes (DEG) were identified and a gene was considered differentially expressed when the *P* value was less than 0.05. DEGs results were visualized using EnhancedVolcano package (1.10.0). ClusterProfiler (4.0.5) was used for gene annotation and gene enrichment. Gene set enrichment scores and *P* values were computed with fGSEA (1.18.0), a fast algorithm for Gene Set Enrichment Analysis (GSEA). The signature genes of Tr1 cells have been reported in previous studies[24,39]. GSEA results were visualized using plotEnrichment function in fGSEA R package.

Co-culture of DCs and T cells and Cytokine measurements

2×10^5 sorted T cells were co-cultured with $0.75\sim1 \times 10^5$ BMDCs in the presence of intact casein protein (Sigma-Aldrich, C8654) or digested casein protein (50 ug/mL). The *in vitro* protein digestion method was modified from a previously reported method[40]. In brief, after the protein suspension temperature was stabilized at 37 °C, the pH was adjusted to 8.0 using NaOH or HCl. Trypsin (Sigma-Aldrich, T0303) at a working concentration of 0.1 mg/mL was added to the protein suspension and incubated for 5 min. Then an equal amount of trypsin inhibitor (Sigma-Aldrich, T9128) was added. Cell culture supernatants were harvested after 24 h of co-culture and stored at −20°C until the cytokine assays. The concentration of IFN-γ,TNF-α, IL-13, IL-5, IL-4, IL-2, IL-6, IL-9, IL-10, IL-17A, IL-17F and IL-22 in supernatants was measured by The Mouse Th Cytokine Panel (12-plex) LEGENDplex Multi-analyte Flow Assay kit (BioLegend, 741044) according to the manufacturer's protocol. CytoFlex S (Beckman Coulter) was used to analyse the beads in the cytokine kit. The fcs data were analyzed by an online software (biolegend.com/enus/immunoassays/legendplex/support/software) provided by manufacturer.

BMDCs

BMDCs from C57BL/6 mice were cultured on 10 cm non-treated cell culture Petri dishes in RPMI with 10% FBS, 20 ng/mL GM-CSF (Biolegend, 576308) and 100 U/mL penicillin–streptomycin (Gibco, 10378016). Every 1–2 days for the first 4 days, plates were gently washed and non-adherent

granulocytes removed by aspirating 50% of the culture media with subsequent replacement of fresh media. On day 4, media were aspirated completely and replaced with fresh culture media with 20 ng/mL GM-CSF. On day 6, BMDC plates were washed with PBS and loosely adherent and non-adherent cells were collected. Cells were centrifuged at 500× *g* for 5 min, resuspended in fresh culture media and replated on 10 cm non-treated cell culture Petri dishes. On days 7–8, plates were washed with PBS and loosely adherent and non-adherent cells were collected.

TCR cloning

Partial sequences of the most abundant TCRs in the TCR repertoires of Tr1 cells and Treg cells were obtained from single-cell TCR sequencing data. Tcrdist3 (0.1.0) was used to calculate distance between each TCR to remove highly similar TCRs in our TCR sequencing data. Full-length sequence of the TCR was obtained using the V-QUEST tool and Gene database provided by IMGT (imgt.org/).

To reconstitute TCRs, cDNA of TCRα and TCRβ were linked with the self-cleavage sequence of 2A (TCRα-p2A-TCRβ), and shuttled into a modified MIGR1 retrovector in which IRES-GFP was replaced with IRES-Thy1.1. Briefly, the target DNA sequence and the DNA oligo primers were synthesized from Qingke (For Cb4-7 TCR: forward, 5'-GGCGCCGGAATTAGATCTCTCGAGGCCACCATGGACAAGATCCTGA-3'; reverse, 5'-AACGTTAGGGGGGGGGGCGGAATTCAGGAATTTTTTTTCTTGACCAT-3'). The target DNA fragment was amplified by PCR using 2× Phanta Max Master Mix (Vazyme, P515-02). The vector plasmid was digested with *Xho* I (NEB, R0146S) and *EcoR* I (NEB, R3101S). The DNA fragments were size-verified by gel electrophoresis. The DNA fragments were purified with Gel Extraction Kit (CWBIO, CW2302M) following the manufacturer's instructions. The DNA fragments were assembled using Exnase MultiS (Vazyme, C113-01). 5 μL of the recombinant plasmid was added to 50 μL of DH5α Competent *E. coli* Cells (Qingke, DLC101) and incubated on ice for 30 min. The mixture was heat-shocked at 42 °C for 60 sec, followed by incubation on ice for 5 min. The bacterial suspension was spread onto Amp^+ LB plates and incubated at 37 °C for 12 h. Single colony was picked and subjected to PCR amplification for verification using Rapid Taq Master Mix (Vazyme, P222-01). The correct single colony was inoculated into 15 mL of liquid LB medium and cultured overnight in a 37 °C shaking incubator. The bacterial culture was centrifuged at 3,000 rpm for 10 min and plasmid DNA was extracted using the Plasmid Midi Preparation Kit (TIANGEN, DP106-02) the following day.

Generation of TCR hybridomas

8 μg of TCR-MIGR1-Thy1.1 plasmid and 8 μg of pCL-Eco plasmid were added to Opti-MEM (total volume of 500μL) in a sterile tube and gently pipetted. 64 μg PEI (2 μg/mL, Polysciences) was added to 468 μL Opti-MEM and mixed thoroughly. The PEI/Opti-MEM mixture was added dropwise to the DNA/Opti-MEM mixture, mixed by pipetting, and incubated at room temperature for 15 min. The PEI/DNA mixture was added dropwise to 293T cells at 50–70% confluency. The plate was gently swirled and incubated at 37 °C for 5 h. The medium was replaced with fresh complete DMEM and incubated at 37 °C for 24 h. The DMEM was replaced with T cell culture medium (TCM). TCM was prepared by supplementing 445 mL RPMI-1640 (Gibco, 11875093) with 50 mL FBS, 5 mL penicillin-streptomycin (Gibco, 10378016), and 500 μL of 55 mM 2-mercaptoethanol (Gibco, 21985023). 293T were cultured for an additional 24 h. TCM containing virus was then collected.

Polybrene was added to the collected TCM (8 μg/mL). NFAT-GFP $58\alpha^-\beta^-$ hybridoma cells (1×10^6) were resuspended in 2 mL of TCM containing 8 μg/mL polybrene. The cells were plated in a 6-well plate and centrifuged at 2,000× *g* for 2 h at 33 °C. The cells were gently resuspended by pipetting and incubated at 37 °C for 2 h. Cells were centrifuged at 800 rpm for 5 min at 4 °C and cultured in 2 mL of fresh prewarmed TCM medium for 48 h.

Then the hybridomas were transferred to a 15 mL Falcon tube and centrifuged at 800 rpm for 5 min at 4 °C. The pellet was resuspended in 200 μL antibody mixture (0.8 μL PE/Cy7-CD4 (GK1.5, Biolegend, 100422), 0.8 μL APC-TCRβ (H57-597, Biolegend, 109212) in 200 μL MACS buffer) and incubated for 15 min at 4 °C. Hybridomas were washed with 5 mL PBS and centrifuged at 800 rpm for 5 min at 4 °C. The pellet was resuspended in 500 μL MACS buffer, and transferred to FACS tubes. Cells were stained with 2.5 μL DAPI (Biolegend, 422801), thoroughly mixed, and sorted for $DAPI^-/CD4^+/TCR\beta^+$ populations, followed by culture.

Hybridoma activation

Splenic dendritic cells were used as antigen-presenting cells (APCs). C57BL/6 mice were injected intraperitoneally with 5×10^6 FLT3L-expressing B16 melanoma cells to drive APC proliferation. Splenocytes were prepared 10–14 days after injection, and positively enriched for $CD11c^+$ cells using Mouse CD11c Positive Selection Kit (STEMCELL, 18780). 2×10^4 hybridoma cells were incubated with 10^5 APCs and antigens in round bottom 96-well plates for two days. Cells were centrifuged at 800× *g* for 5 min at 4 °C and the pellet was resuspended in 50 μL antibody mixture (0.2 μL PE-Thy1.1 (OX-7, Biolegend, 202524), 0.2 μL APC-TCRβ in MACS buffer) and incubated for 15 min at 4°C. Cells were washed with 200 μL PBS and centrifuged at 800 rpm for 5 min at 4 °C. The pellet was resuspended in 200 μL MACS buffer, and transferred to FACS tubes. Cells were stained with 1 μL DAPI (200×), thoroughly mixed. GFP induction in the $DAPI^-/Thy1.1^+/TCR\beta^+$ hybridomas was analysed by flow cytometry as an indicator of TCR activation.

IECs fixation

The method of IEC fixation has been described in previous studies[14]. In brief, IECs were sorted into PBS solution containing 1% PFA using vertical sorting mode, and the fixed cells were then washed twice with PBS containing 200 mM glycine. IECs were then resuspended in X-VIVO 20 medium and co-cultured with T cells. After 2×10^6 IECs and 2×10^5 T cells were co-cultured for 12 h, the cells were collected for subsequent analysis.

Generation of TCR transgenic mice

Cb4-7 TCRα and TCRβ sequences of were cloned into the pTα and pTβ vectors provided by D. Mathis, respectively. TCR

transgenic mice were generated by the the animal facility at USTC. Positive pups were genotyped by testing TCR Vβ8.1/8.2 expression on T cells from peripheral blood.

Synthetic peptides

Synthetic peptides representing antigens presented by IECs for hybridoma activation assays were synthesized by and purchased from Top-peptide (Shanghai). All peptides were above or equal to 95% purity (HPLC).

Tetramer staining

~1 × 10^6 sorted T cells were stained by PE and APC-conjugated Cb_{98-112}:I-A^b tetramers at 37 °C for 2 h in the dark. Then cells were washed twice and enriched using anti-PE beads (Miltenyi Biotec) and anti-APC beads (Miltenyi Biotec). The enriched T cells were stained with Zombie Aqua™ dye as described above and analyzed by flow cytometry.

Cell transfer

Single cells were collected from pooled spleens and lymph nodes of 8–10 week CD45.1 Cb4-7 Tg IL-10^{GFP}/$FOXP3^{RFP}$ dual reporter mice. Naïve $CD4^+$ T cells were isolated by negative magnetic selection (Biolegend) according to the manufacturer's protocols. Isolated naïve $CD4^+$ T cells were transferred into CD45.2 IL-10^{GFP}/$FOXP3^{RFP}$ dual reporter mice or *H2-Ab1*$^{\Delta IEC}$, *H2-Ab1*$^{\Delta DC}$ and *H2-Ab1*$^{\Delta B}$ mice crossed with IL-10^{GFP}/$FOXP3^{RFP}$ dual reporter mice by intravenous injection (1 × 10^6 per mouse).

Preparation of Casein-FITC, Casein, OVA or PN peptides-loaded PGNPs

PGNPs were prepared as previously described[34]. For Casein-FITC- or OVA-loaded PGNPs, 330 µL of Casein-FITC (3 mg/mL in Milli-Q water) or 200 µL of OVA (6 mg/mL in Milli-Q water) was added to 0.5 mL dichloromethane solution, emulsified by sonication, and washed three times with Milli-Q water using an ultrafiltration tube to remove unbound peptides. The final concentration of peptide loaded by PGNPs was determined using a spectrophotometer.

To generate PGNPs loaded with casein or PN epitopes, each of the 8 casein peptides (3 mg/mL in Milli-Q water) or 8 PN peptides (2 mg/mL in Milli-Q water) was individually processed: 200 µL of peptide solution was emulsified with 0.5 mL dichloromethane by sonication, followed by three washes with Milli-Q water via ultrafiltration to remove unbound peptides. This yielded 8 distinct PGNPs preparations per peptide set (casein or PN) for subsequent *in vivo* experiments. The final concentration of peptide loaded by PGNPs was determined using a spectrophotometer.

Measurement of the delivery efficiency of PGNPs to IECs

The delivery efficiency of PGNPs to intestinal epithelial cells was assessed by orally administering Casein-FITC-loaded PGNPs (2 mg per mouse) to mice, with free Casein-FITC peptides serving as the control (2 mg per mouse). At 1, 4, 8, and 12 h post-gavage, mice were euthanized and the proximal/distal small intestine and colon were collected for IEC isolation. The obtained IECs, which were then stained with anti-EpCAM-APC and analyzed by flow cytometry to quantify $FITC^+EpCAM^+$ live IECs. Fluorescence intensity was measured in the FITC channel to compare PGNPs-mediated delivery versus free peptide uptake across different intestinal segments and time points.

In vivo sensitization, intervention and challenge

BALB/c (4 weeks old females) were acclimatized for 2 weeks before experiment. For CT (Sigma-Aldrich)/PE model, BALB/c mice were orally sensitized with PBS (sham-sensitization, naïve group), or PN extract (6 mg per dose) and CT (10 µg per dose) in 200 µL PBS on days 0, 1, 2, 7, 14, 21, and 28. From day 28, these mice were orally administered with PBS, PGNPs, free PN peptides or PGNPs-peptides for 21 days (2 times per day, free PN peptides: 0.2 mg per dose; PGNPs-peptides: 0.2 mg per dose). Naïve mice were orally administered with PBS as a control. On day 49, mice were i.p. injected with 1 mg PE and the body temperature was recorded.

For mMCP-1 detection: Serum samples were collected 80 min post-challenge. mMCP-1 was detected following the instructions of the commercial Mouse MCPT 1 (mMCP 1) ELISA kit (Invitrogen, 88-7503-88).

For allergen-specific IgE and IgG detection: Serum samples were collected 24 h post-challenge. PN allergen-specific antibody in serum was detected via enzyme-linked immunosorbent assay (ELISA) method. Briefly, the 96-well ELISA plate was coated with 50 µg/mL of PN extracts in 100 mM carbonate-bicarbonate buffer (pH 9.6) per well and incubated overnight at 4 °C. The plate was washed four times and blocked with 1% BSA in PBS buffer for 2 h. After washing, serum samples were diluted (1:10 diluent for IgE and 1:500 diluent for IgG) and incubated in 96-well plate overnight at 4 °C. After repeated washing, horseradish peroxidase (HRP)-conjugated goat anti-mouse IgE and IgG (1:4,000 dilution, SouthernBiotech) were added to each well and incubated for 1 h. The plate was thoroughly washed and 100 µL of 3,3',5,5'-tetramethylbenzidine (TMB) solution was added to each well. 15 min later, the stop solution (1 M H_2SO_4) was added and the optical density (OD) value at 450 nm was measured via a microplate reader.

DQ-Ovalbumin degradation assay

IEC preparation: small intestines were excised, flushed three times with PBS, and turned inside out. The tissue was cut into 1 cm sections and incubated in RPMI 1640 containing 2 mM EDTA and 2% FBS for 15 min at 37 °C with shaking. Supernatants were passed through a 100 µm cell strainer to obtain single-cell suspensions. Cells were collected as the IEC fraction. DC preparation: bone marrow cells were harvested from 8-week-old wild-type mice. Red blood cells were lysed with ACK buffer, and the remaining cells were cultured at 5 × 10^6 cells/mL in RPMI 1640 medium supplemented with 10% FBS, 50 ng/mL Flt3L, 0.1 mM NEAA, 1 mM sodium pyruvate, 2 mM GlutaMAX, 100 U/mL penicillin, 100 µg/mL streptomycin, and 50 µM β-mercaptoethanol. Cells were cultured undisturbed for 9–11 days, after which floating and loosely adherent cells were collected as DCs by vigorous pipetting. DQ-Ovalbumin assay: A total of 5 × 10^5 IECs or DCs were incubated with 10 µg/mL DQ-Ovalbumin (Invitrogen, Cat# D12053) for various time points. Cells were then washed three times with PBS, stained with surface marker antibodies, and analyzed for $FITC^+$ cells by flow cytometry.

Eα preparation and treatment

To evaluate the antigen-presenting capacity of murine intestinal epithelial cells, we utilized the well-established Eα/Y-Ae system as described[41-43]. Recombinant Eα protein was generated as follows: Eα was cloned into the pFastBac HTB vector with an N-terminal TEV-cleavable His_6-MBP tag. The construct was transformed into *E. coli* DH10Bac for bacmid production. Recombinant baculoviruses were generated and used to infect Sf9 cells for protein expression. Cells were harvested 96 h post infection at 27 °C and lysed by sonication in buffer containing 20 mM Tris-HCl (pH 7.4), 500 mM NaCl, and 20 mM imidazole. Clarified lysates were incubated with Ni-NTA resin, washed with the same buffer, and eluted with 500 mM imidazole. Target proteins were further purified by size exclusion chromatography on a Superdex 200 column to isolate monomeric fractions. Eα DNA sequence:

5'-atgggggcgatggctccgcgcacgctgctcctgctgctggcggccgccctggccccgactcagacccgcgcgggcccacactcgatgcggtatttcgagaccgccgtgtccccggcccggcctcgaggagccccggtacatctctgtcggctatgtggacaacaaggagttcgtgcgcttcgacagcgacgcggagaatccgagatatgagccgcgggcgccgtggatggagcaggaggggccggagtattgggagcgggaaacacagaaagccaagggccaagagcagtggttccgagtgagcctgaggaacctgctcggctactacaaccagagcgcgggcggctctcacacactccagcagatgtctggctgtgacttggggtcggactggcgcctcctccgcgggtacctgcagttcgcctatgaaggccgcgattacatcgccctgaacgaagacctgaaaacgtggacggcggcggacatggcggcgcagatcacccgacgcaagtgggagcagagtggtgctgcagagcattacaaggcctacctggagggcgagtgcgtggagtggctccacagatacctgaagaacgggaacgcgacgctgctgcgcacagattccccaaaggcacatgtgacccatcaccccagatctaaaggtgaagtcaccctgaggtgctgggccctgggcttctaccctgctgacatcaccctgacctggcagttgaatggggaggagctgacccaggacatggagcttgtggagaccaggcctgcaggggatggaaccttccagaagtgggcatctgtggtggtgcctcttgggaaggagcagaattacacatgccgtgtgtaccatgaggggctgcctgagcccctcaccctgagatgggagcctcctccgtccactgactcttacatggtgatcgttgctgttctgggtgtccttggagctatggccatcattggagctgtggtggctttttgtgatgaagagaaggagaaacacaggtggaaaaggaggggactatgctctggctccaggctcccagagctctgaaatgtctctccgagattgtaaagcgtga-3'

The Eα 52–68 peptide was obtained from ANASPEC, and the Y-Ae monoclonal antibody (specific for I-Ab complexed with Eα peptide) was purchased from eBioscience (11-5741-82). Murine small intestinal epithelial cells were cultured in 96-well plates and treated with either Eα protein or Eα 52–68 peptide at a concentration of 100 μg/mL. After 4 h of incubation, cells were harvested for immunofluorescence analysis.

Statistical analysis

Data analysis was processed and represented by GraphPad Prism 9. Statistical significance was determined by two-sided Student's *t*-test, one-way ANOVA Dunnett's multiple comparisons test, one-way ANOVA Tukey's multiple comparisons test and two-way ANOVA Šídák's multiple comparisons, as indicated in figure legends. A *P* value of less than 0.05 (confidence interval of 95%) was considered significant. NS, no significance; $*P < 0.05$; $**P < 0.01$; $***P < 0.001$ and $****P < 0.0001$. The sample sizes are stated in the figure legends to indicate biologically independent replicates used for statistical analysis.

DATA AVAILABILITY

The single-cell RNA and TCR sequencing data and the bulk RNA-seq data have been deposited in the Genome Sequence Archive at BIG Data Center, Beijing Institute of Genomics (BIG), Chinese Academy of Sciences. Project number is PRJCA049178. All other data supporting the findings of this study are available from the corresponding authors upon reasonable request.

ACKNOWLEDGMENT

We thank Mo Xu from National Institute of Biological Sciences for providing the vectors used to produce the TCR transgenic mice, the 58α$^-$β$^-$T cell hybridoma cell line, and the MIGR1-Thy1.1 plasmid. We thank Jincun Zhao from Guangzhou Medical University for the assistance provided during the production of TCR transgenic mice. We thank Rongbin Zhou for providing *Vil1-Cre*, *CD11c-gfp-Cre* mice. We thank Wen Pan for providing *Vil1*^{CreERT2} mice. We thank Mengjie Liu and Hong Yao for their help in animal experiments. We thank Jian Wang and members of his laboratory for advice and assistance with T cell factor assays. We thank Hai Li and members of his laboratory for assistance with TCR cloning. This work was supported by grants from the National Natural Science Foundation of China (92374204, 82325025, 82588302, 82341121), the CAS Project for Young Scientists in Basic Research (YSBR-074), the Strategic Priority Research Program of the Chinese Academy of Sciences (XDB0940303).

AUTHOR CONTRIBUTIONS

S.Z. and T.Z. conceived the project and designed the experiments. T.Z., G.Z., and C.W. performed the experiments and collected the data. T.Z. analyzed the single-cell and bulk RNA-seq data. Yan.W. conducted experiments assessing IEC antigen presentation function. T.W. and R.L. assisted with animal experiments. W.J. and Yucai.W. prepared PGNP-peptide nanoparticles. S.Z. and T.Z. wrote the manuscript. G.Z. and A.J.M. revised the manuscript. S.Z. supervised the project.

COMPETING INTERESTS

S.Z. is a cofounder of Ibiome which studies microbial regulation of immune responses in topics unrelated to the subject of this work.

REFERENCES

1. Renz, H. et al. Food allergy. *Nat. Rev. Dis. Primers* **4**, 17098 (2018).
2. Pabst, O. & Mowat, A.M. Oral tolerance to food protein. *Mucosal Immunol.* **5**, 232–239 (2012).
3. Mazzini, E., Massimiliano, L., Penna, G. & Rescigno, M. Oral tolerance can be established via gap junction transfer of fed antigens from CX3CR1$^+$ macrophages to CD103$^+$ dendritic cells. *Immunity* **40**, 248–261 (2014).
4. Schulz, O. et al. Intestinal CD103$^+$, but not CX3CR1$^+$, antigen sampling cells migrate in lymph and serve classical dendritic cell functions. *J. Exp. Med.* **206**, 3101–3114 (2009).
5. Esterházy, D. et al. Classical dendritic cells are required for dietary antigen-mediated induction of peripheral T_{reg} cells and tolerance. *Nat. Immunol.* **17**, 545–555 (2016).
6. Campos Canesso, M.C. et al. Identification of antigen-presenting cell-T cell interactions driving immune responses to food. *Science* **387**, eado5088 (2025).
7. Fu, L.H. et al. PRDM16-dependent antigen-presenting cells induce tolerance to gut antigens. *Nature* **642**, 756–765 (2025).

8. Rodrigues, P.F. et al. Rorγt-positive dendritic cells are required for the induction of peripheral regulatory T cells in response to oral antigens. *Cell* **188**, 2720–2737.e22 (2025).
9. Cabric, V. et al. A wave of Thetis cells imparts tolerance to food antigens early in life. *Science* **389**, 268–274 (2025).
10. Koyama, M. et al. MHC class II antigen presentation by the intestinal epithelium initiates graft-versus-host disease and is influenced by the microbiota. *Immunity* **51**, 885–898.e7 (2019).
11. Tuganbaev, T. et al. Diet diurnally regulates small intestinal microbiome-epithelial-immune homeostasis and enteritis. *Cell* **182**, 1441–1459.e21 (2020).
12. Westendorf, A.M. et al. $CD4^{+}Foxp3^{+}$ regulatory T cell expansion induced by antigen-driven interaction with intestinal epithelial cells independent of local dendritic cells. *Gut* **58**, 211–219 (2009).
13. Biton, M. et al. T helper cell cytokines modulate intestinal stem cell renewal and differentiation. *Cell* **175**, 1307–1320.e22 (2018).
14. He, K.X. et al. Gasdermin D licenses MHCII induction to maintain food tolerance in small intestine. *Cell* **186**, 3033–3048.e20 (2023).
15. Bilate, A.M. et al. T cell receptor is required for differentiation, but not maintenance, of intestinal $CD4^{+}$ intraepithelial lymphocytes. *Immunity* **53**, 1001–1014.e20 (2020).
16. Lockhart, A. et al. Dietary protein shapes the profile and repertoire of intestinal $CD4^{+}$ T cells. *J. Exp. Med.* **220**, e20221816 (2023).
17. Hong, S.W. et al. Immune tolerance of food is mediated by layers of $CD4^{+}$ T cell dysfunction. *Nature* **607**, 762–768 (2022).
18. Curotto de Lafaille, M.A. et al. Adaptive $Foxp3^{+}$ regulatory T cell-dependent and -independent control of allergic inflammation. *Immunity* **29**, 114–126 (2008).
19. Hadis, U. et al. Intestinal tolerance requires gut homing and expansion of $FoxP3^{+}$ regulatory T cells in the lamina propria. *Immunity* **34**, 237–246 (2011).
20. Kim, K.S. et al. Dietary antigens limit mucosal immunity by inducing regulatory T cells in the small intestine. *Science* **351**, 858–863 (2016).
21. Sujino, T. et al. Tissue adaptation of regulatory and intraepithelial $CD4^{+}$ T cells controls gut inflammation. *Science* **352**, 1581–1586 (2016).
22. Maynard, C.L. et al. Regulatory T cells expressing interleukin 10 develop from $Foxp3^{+}$ and $Foxp3^{-}$ precursor cells in the absence of interleukin 10. *Nat. Immunol.* **8**, 931–941 (2007).
23. Huber, S. et al. Th17 cells express interleukin-10 receptor and are controlled by $Foxp3^{-}$ and $Foxp3^{+}$ regulatory $CD4^{+}$ T cells in an interleukin-10-dependent manner. *Immunity* **34**, 554–565 (2011).
24. Sultan, H. et al. Neoantigen-specific cytotoxic Tr1 CD4 T cells suppress cancer immunotherapy. *Nature* **632**, 182–191 (2024).
25. Yu, H. et al. Intestinal type 1 regulatory T cells migrate to periphery to suppress diabetogenic T cells and prevent diabetes development. *Proc. Natl. Acad. Sci. USA* **114**, 10443–10448 (2017).
26. Clemente-Casares, X. et al. Expanding antigen-specific regulatory networks to treat autoimmunity. *Nature* **530**, 434–440 (2016).
27. Ansaldo, E. et al. T-bet-expressing Tr1 cells driven by dietary signals dominate the small intestinal immune landscape. *Proc. Natl. Acad. Sci. USA* **123**, e2520747122 (2026).
28. Kalekar, L.A. et al. $CD4^{+}$ T cell anergy prevents autoimmunity and generates regulatory T cell precursors. *Nat. Immunol.* **17**, 304–314 (2016).
29. Gagliani, N. et al. Th17 cells transdifferentiate into regulatory T cells during resolution of inflammation. *Nature* **523**, 221–225 (2015).
30. Roncarolo, M.G., Gregori, S., Bacchetta, R., Battaglia, M. & Gagliani, N. The biology of T regulatory type 1 cells and their therapeutic application in immune-mediated diseases. *Immunity* **49**, 1004–1019 (2018).
31. Vita, R. et al. The immune epitope database (IEDB): 2018 update. *Nucleic Acids Res.* **47**, D339–D343 (2019).
32. Reynisson, B., Alvarez, B., Paul, S., Peters, B. & Nielsen, M. NetMHCpan-4.1 and NetMHCIIpan-4.0: improved predictions of MHC antigen presentation by concurrent motif deconvolution and integration of MS MHC eluted ligand data. *Nucleic Acids Res.* **48**, W449–W454 (2020).
33. London, M., Bilate, A.M., Castro, T.B.R., Sujino, T. & Mucida, D. Stepwise chromatin and transcriptional acquisition of an intraepithelial lymphocyte program. *Nat. Immunol.* **22**, 449–459 (2021).
34. Zhang, G.R. et al. Glucosylated nanoparticles for the oral delivery of antibiotics to the proximal small intestine protect mice from gut dysbiosis. *Nat. Biomed. Eng.* **6**, 867–881 (2022).
35. Lyu, M.Z. et al. ILC3s select microbiota-specific regulatory T cells to establish tolerance in the gut. *Nature* **610**, 744–751 (2022).
36. Awasthi, A. et al. A dominant function for interleukin 27 in generating interleukin 10-producing anti-inflammatory T cells. *Nat. Immunol.* **8**, 1380–1389 (2007).
37. Jones, S.M. et al. Efficacy and safety of oral immunotherapy in children aged 1-3 years with peanut allergy (the Immune Tolerance Network IMPACT trial): a randomised placebo-controlled study. *Lancet* **399**, 359–371 (2022).
38. Hunter, H. et al. Oral immunotherapy in peanut-allergic adults using real-world materials. *Allergy* **80**, 2310–2318 (2025).
39. Zhang, H.Y. et al. An IL-27-driven transcriptional network identifies regulators of IL-10 expression across T helper cell subsets. *Cell Rep.* **33**, 108433 (2020).
40. Brodkorb, A. et al. INFOGEST static in vitro simulation of gastrointestinal food digestion. *Nat. Protoc.* **14**, 991–1014 (2019).
41. Pape, K.A., Catron, D.M., Itano, A.A. & Jenkins, M.K. The humoral immune response is initiated in lymph nodes by B cells that acquire soluble antigen directly in the follicles. *Immunity* **26**, 491–502 (2007).
42. Rush, C.M., Mitchell, T.J. & Garside, P. A detailed characterisation of the distribution and presentation of DNA vaccine encoded antigen. *Vaccine* **28**, 1620–1634 (2010).
43. Macritchie, N. et al. Plasmacytoid dendritic cells play a key role in promoting atherosclerosis in apolipoprotein E-deficient mice. *Arterioscler. Thromb. Vasc. Biol.* **32**, 2569–2579 (2012).

ADDITIONAL INFORMATION

Supplementary information The online version contains supplementary material available at https://doi.org/10.15302/vita.2026.08.0066.

Correspondence and requests for materials should be addressed to Shu Zhu

Reprints and permission information is available at https://www.vita-journal.com/.

© The Author(s) 2026. Published by Higher Education Press. This is an Open Access article distributed under the terms of the CC BY license (https://creativecommons.org/licenses/by/4.0/).